

## RESEARCH ARTICLE

# $\alpha$ -Catenin phosphorylation promotes intercellular adhesion through a dual-kinase mechanism

David J. Escobar<sup>1,2,\*</sup>, Ridhdhi Desai<sup>3,\*</sup>, Noboru Ishiyama<sup>4</sup>, Stephen S. Folmsbee<sup>1,2</sup>, Megan N. Novak<sup>1,2</sup>, Annette S. Flozak<sup>1</sup>, Rebecca L. Daugherty<sup>1,2</sup>, Rigen Mo<sup>1</sup>, Dhaval Nanavati<sup>5</sup>, Ritu Sarpal<sup>3</sup>, Deborah Leckband<sup>6</sup>, Mitsu Ikura<sup>4</sup>, Ulrich Tepass<sup>3,‡</sup> and Cara J. Gottardi<sup>1,7,‡</sup>

**ABSTRACT**

The cadherin–catenin adhesion complex is a key contributor to epithelial tissue stability and dynamic cell movements during development and tissue renewal. How this complex is regulated to accomplish these functions is not fully understood. We identified several phosphorylation sites in mammalian  $\alpha$ E-catenin (also known as catenin  $\alpha$ -1) and *Drosophila*  $\alpha$ -Catenin within a flexible linker located between the middle (M)-region and the carboxy-terminal actin-binding domain. We show that this phospho-linker (P-linker) is the main phosphorylated region of  $\alpha$ -catenin in cells and is sequentially modified at casein kinase 2 and 1 consensus sites. In *Drosophila*, the P-linker is required for normal  $\alpha$ -catenin function during development and collective cell migration, although no obvious defects were found in cadherin–catenin complex assembly or adherens junction formation. In mammalian cells, non-phosphorylatable forms of  $\alpha$ -catenin showed defects in intercellular adhesion using a mechanical dispersion assay. Epithelial sheets expressing phosphomimetic forms of  $\alpha$ -catenin showed faster and more coordinated migrations after scratch wounding. These findings suggest that phosphorylation and dephosphorylation of the  $\alpha$ -catenin P-linker are required for normal cadherin–catenin complex function in *Drosophila* and mammalian cells.

**KEY WORDS:**  $\alpha$ -catenin, Adhesion, Migration, Phospho-regulation

**INTRODUCTION**

Adherens junctions are cell contact sites of actin protein enrichments that play a fundamental role in coordinating collective cell behaviors in developing and homeostatic tissues (reviewed in Halbleib et al., 2007; Harris and Tepass, 2010; Nishimura and Takeichi, 2009). Whereas numerous studies

support the pre-eminent role of cadherins and their associated catenins in adherens junction structure and function in cell culture systems and multiple metazoan model species, we know comparatively little about the signals and modifications that regulate the cadherin–catenin complex (CCC), and what comprises strong and weak adhesion at the molecular level.

As the sole actin-binding component of the CCC, there is much interest in how  $\alpha$ -catenin engages the filamentous (F)-actin cytoskeleton to allow for both static and dynamic cell–cell adhesion. Cells contain two pools of  $\alpha$ -catenin, a cadherin– $\beta$ -catenin associated pool and a cytosolic cadherin-free pool (Drees et al., 2005; Schneider et al., 1993). The cytosolic pool of  $\alpha$ -catenin can affect actin dynamics, such as limiting Arp2/3-based actin polymerization and severing by cofilin (Benjamin et al., 2010; Drees et al., 2005; Hansen et al., 2013). By contrast, the cadherin– $\beta$ -catenin bound pool of  $\alpha$ -catenin is crucial for adherens junctions, and links the cadherin– $\beta$ -catenin complex and the actin cytoskeleton in support of normal cell adhesion (Desai et al., 2013).

The view that  $\alpha$ -catenin plays a key role within the CCC is reinforced by evidence that  $\alpha$ -catenin behaves as a mechanosensor (Barry et al., 2014; le Duc et al., 2010; Yonemura et al., 2010), where actomyosin-force-generated tension leads to unfolding of an auto-inhibited middle (M)-region that allows binding to the  $\alpha$ -catenin and F-actin-binding protein vinculin (Choi et al., 2012; Ishiyama et al., 2013; le Duc et al., 2010; Rangarajan and Izard, 2013; Yao et al., 2014; Yonemura et al., 2010). Evidence that the M-domain can bind to a number of F-actin-binding proteins (e.g. afadin,  $\alpha$ -actinin; Kobiela and Fuchs, 2004; Maiden and Hardin, 2011) suggests a model where tension might cause  $\alpha$ -catenin to unfold and recruit diverse F-actin-binding proteins leading to cell-type and context-dependent reinforcement of adherens junctions. How cell signaling events enhance or antagonize the mechanosensitivity of  $\alpha$ -catenin is unknown. Previous work has indicated that  $\alpha$ -catenin present within the CCC can undergo phosphorylation (Burks and Agazie, 2006; Chen et al., 2009; Dupre-Crochet et al., 2007; Ji et al., 2009; Stappert and Kemler, 1994), but the identification of key sites and their functional significance has remained largely unexplored. Here, we identify a highly conserved phospho-domain in  $\alpha$ -catenin that contributes to intercellular adhesion in mammalian cells and *Drosophila* through a dual-kinase mechanism.

**RESULTS****Identification of a major serine/threonine phospho-domain in  $\alpha$ -catenin**

To identify phosphorylation sites in  $\alpha$ E-catenin ( $\alpha$ E-cat, also known as catenin  $\alpha$ -1) we affinity purified cadherin-free

<sup>1</sup>Department of Medicine, Northwestern University Feinberg School of Medicine, Chicago, IL 60611, USA. <sup>2</sup>The Driskill Graduate Training Program in Life Sciences, Northwestern University Feinberg School of Medicine, Chicago, IL 60611, USA. <sup>3</sup>Department of Cell and Systems Biology, University of Toronto, Toronto, ON, M5S 3G5 Canada. <sup>4</sup>University Health Network, Princess Margaret Cancer Center, University of Toronto, Toronto, ON M5T 2M9, Canada.

<sup>5</sup>Department of Chemistry of Life Processes, Northwestern University Feinberg School of Medicine, Chicago, IL 60611, USA. <sup>6</sup>Department of Chemical and Biomolecular Engineering, University of Illinois, Urbana, IL 61801, USA.

<sup>7</sup>Department of Cellular and Molecular Biology, Northwestern University Feinberg School of Medicine, Chicago, IL 60611, USA.

\*These authors contributed equally to this work

‡Authors for correspondence (u.tepass@utoronto.ca; c-gottardi@northwestern.edu)

$\alpha$ E-cat- and  $\beta$ -catenin-containing complexes from human colon-cancer-derived SW480 cells and analyzed them with high mass accuracy electrospray tandem mass spectrometry (LC-MS/MS) and nano-electrospray tandem mass spectrometry in collaboration with the Taplin facility (Harvard University, Cambridge, MA) (Fig. 1A–C). Four clustered phosphorylated serine (Ser, S) and threonine (Thr, T) residues were identified that localize to a flexible linker region (amino acids 631–661) between the M-region and the C-terminal F-actin-binding domain of  $\alpha$ E-cat (Ishiyama et al., 2013; Rangarajan and Izard, 2013; Yonemura et al., 2010). These sites were previously identified in other large-scale phosphoproteomic screens, where S641 is the most commonly observed site (mouse – Ballif et al., 2004; Huttlin et al., 2010; human – Beausoleil et al., 2004; Dephoure et al., 2008; Olsen et al., 2006). These sites appear to be responsible for most [ $^{32}$ P]orthophosphate labeling of cellular  $\alpha$ E-cat, particularly S641 (Fig. 2M).

Multiple sequence alignment of  $\alpha$ -catenin proteins from diverse species indicates a conservation of the Ser and Thr residues in the linker between the M- and C-terminal (C)-domains (Fig. 1D,E). Moreover, phosphoproteomic screens in *Drosophila* identified seven possible phosphorylated Ser and Thr residues in this region, including T645, which likely corresponds to S641 in  $\alpha$ E-cat (Fig. 1E) (Zhai et al., 2008). Taken together, these data support the identification of a major, evolutionarily conserved phospho-domain in  $\alpha$ -catenin proteins that we will refer to as the phospho-linker (P-linker) region.

#### $\alpha$ E-cat is phosphorylated by a hierarchical dual-kinase mechanism

Because mass spectrometry assigns phospho-modified residues imperfectly (Taus et al., 2011) (Fig. 1C), we sought to characterize  $\alpha$ E-cat phosphorylation *in vitro*. To identify potential kinases, we used the bioinformatic tool NetPhos (<http://www.cbs.dtu.dk/services/NetPhosK>). Although this program identified numerous putative kinases that might target the P-linker region, previous inhibitor studies hinted that casein kinases 1 and 2 (CK1 and CK2) might contribute to  $\alpha$ E-cat phosphorylation (Bauer et al., 1998; Dupre-Crochet et al., 2007). Indeed, *in vitro* kinase assays revealed that S641 is the major CK2 site in  $\alpha$ E-cat (Fig. 2A,B; CK2 condition), whereas the Ser/Thr residues between 652 and 658 were the major CK1 sites (Fig. 2C,D; CK1 condition).  $\alpha$ E-cat phosphorylation by CK2 occurred rapidly (i.e. saturated within ~5 minutes), in contrast to CK1 phosphorylation kinetics, which were significantly slower (i.e. increased over 90 minutes) (Fig. 2C,D).

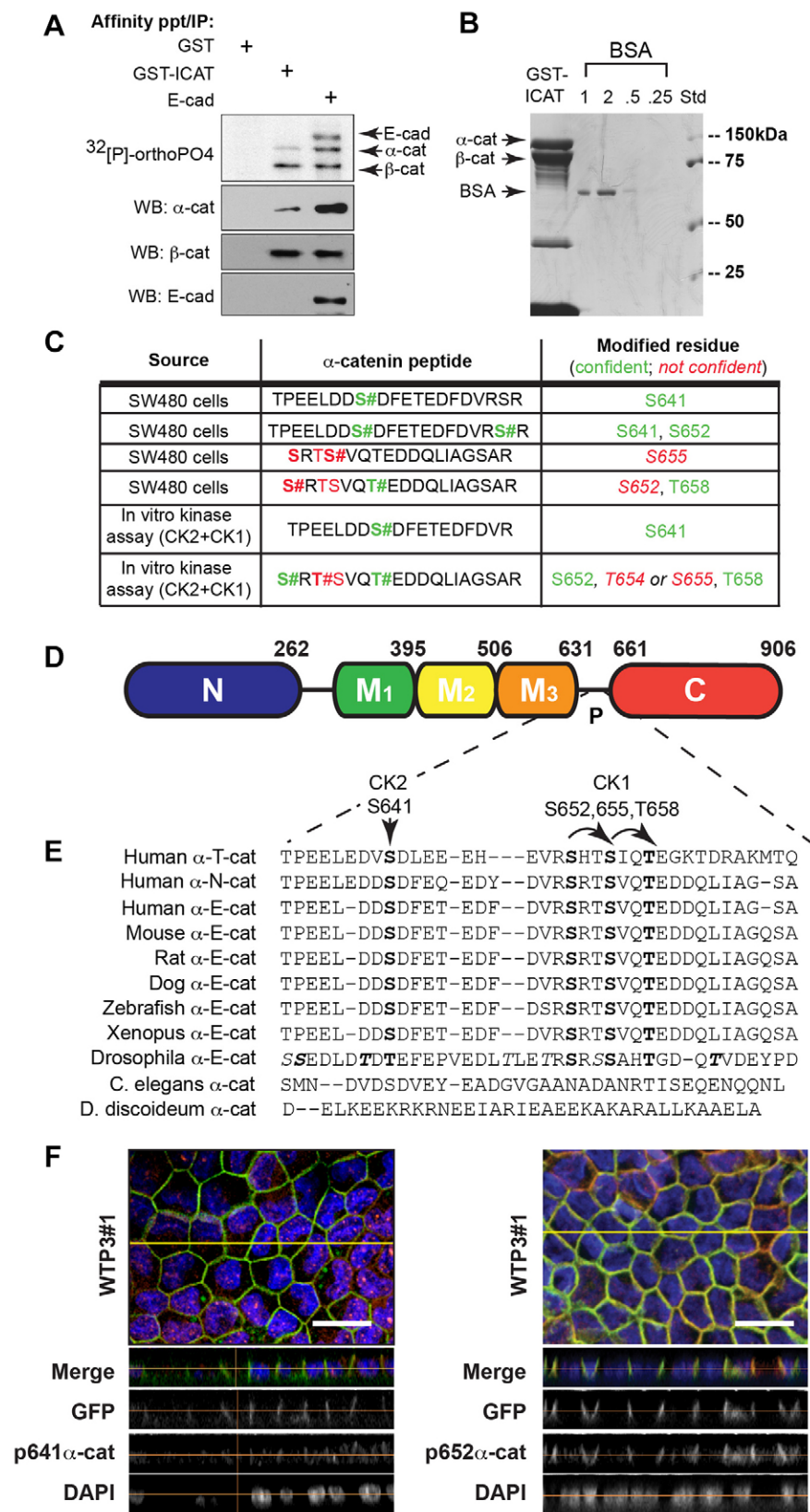
As residues S652, S655, and T658 of  $\alpha$ E-cat conform to a hierarchical CK1 phospho-scheme, which prefers a negatively charged amino acid (aspartate or glutamate, D or E) or phosphorylation at the –3 position (Marin et al., 1994; Pulgar et al., 1999), we sought experimental evidence as to whether this scheme also applies to  $\alpha$ E-cat. We found that mutating the most N-terminal of the three consensus CK1 sites (S652A) reduced  $\alpha$ E-cat phosphorylation by CK1 as effectively as removing all three CK1 sites (Fig. 2E,F; 3A mutant). Moreover, phosphoproteomic analysis of CK1-phosphorylated recombinant  $\alpha$ E-cat detected a peptide with three phosphates (Fig. 1C), although the precise identification of the middle CK1 phosphorylation site could not be confidently assigned using the phosphoRS algorithm (Taus et al., 2011). Because CK1 phosphorylation schemes similar to that depicted in Fig. 2L are well described (Okamura et al., 2004), it is likely that S652, S655 and T658 conform to

a hierarchical CK1-dependent phospho-scheme. Moreover, evidence that  $\alpha$ E-cat phosphorylation by CK1 increases over time, whereas CK2 phosphorylation saturates within the first 5 minutes (Fig. 2C,D), further supports the sequential nature of CK1 phosphorylation of  $\alpha$ E-cat.

The proximity of CK2 and CK1 phosphorylation sites within the P-linker raised the possibility that these phosphorylations might be coordinated. Whereas the loss of the CK1 sites (S652, S655 and T658) did not affect the phosphorylation of  $\alpha$ E-cat at S641 by CK2 (Fig. 2C,D), loss of the CK2 site (S641A) modestly, but reproducibly, reduced  $\gamma$ - $^{32}$ P incorporation at the CK1 sites (Fig. 2A,B), raising the possibility that phosphorylation by CK2 at S641 might promote  $\alpha$ E-cat phosphorylation by CK1. Indeed, a S641D mutant  $\alpha$ E-cat enhanced phosphorylation by CK1 approximately threefold (Fig. 2I,J). How the CK2 phosphorylation event improves phosphorylation by CK1 appears to be related to the accessibility of the CK1 sites in the full-length  $\alpha$ E-cat protein. We found that a fragment of  $\alpha$ E-cat consisting of the C-terminal 447 residues ( $\alpha$ E-cat459-906), which contains the P-linker, incorporates approximately three times more  $\gamma$ - $^{32}$ P than full-length protein in a CK1 kinase assay (Fig. 2G,H). By contrast, no differences in incorporation are observed at the nearby CK2 site. This suggests that CK2 might enhance phosphorylation by CK1 by promoting a conformation of  $\alpha$ E-cat that enhances CK1 accessibility. To address this, we compared the contribution of CK2 modification (S641A or S641D) to subsequent CK1 phosphorylation in both  $\alpha$ E-cat459-906 or full-length  $\alpha$ E-cat. Interestingly, we found that both  $\alpha$ E-cat459-906:S641D and  $\alpha$ E-cat459-906:S641A were moderately better substrates for CK1 compared with the wild-type  $\alpha$ E-cat459-906 (supplementary material Fig. S1B; ~2-fold versus ~1.5-fold increase in  $\gamma$ - $^{32}$ P incorporation, respectively). This was not the case for full-length  $\alpha$ E-cat, where  $\alpha$ E-cat:S641D enhanced CK1 phosphorylation up to fivefold, whereas  $\alpha$ E-cat:S641A consistently reduced CK1 phosphorylation (Fig. 2A,B,I,J). Given that the contributions of S641A and S641D are quantitatively and directionally different between full-length  $\alpha$ E-cat and  $\alpha$ E-cat459-906, we propose that phosphorylation at S641 by CK2 affects the accessibility of the CK1 sites in  $\alpha$ E-cat. Lastly, whereas phosphorylation at S652 in Madin Darby canine kidney (MDCK) cells is sensitive to the CK1 inhibitor D4476, phosphorylation at S641 is not sensitive to the CK2 inhibitor K66 (Fig. 2K). These data suggest that CK1 is a bona fide kinase for  $\alpha$ E-cat, but that either the priming kinase for S641 is not CK2 or S641 is redundantly phosphorylated by other kinases.  $\alpha$ E-cat phosphorylated at S641 and S652 is largely localized to cell–cell contacts (Fig. 1F).

#### The $\alpha$ E-cat phospho-domain contributes to the strength of intercellular adhesion in MDCK cells

To determine the contribution of phosphorylation at the P-linker to  $\alpha$ E-cat function, we examined the activity of non-phosphorylatable and phosphomimetic forms of  $\alpha$ E-cat (Fig. 3A) in MDCK cells. We first expressed GFP-tagged murine wild-type (GFP- $\alpha$ E-cat), non-phosphorylatable (GFP- $\alpha$ E-catS641A; GFP- $\alpha$ E-cat-5A), phosphomimetic (GFP- $\alpha$ E-catS641E; GFP- $\alpha$ E-cat-5E) or deletion of the P-linker (GFP- $\alpha$ E-cat- $\Delta$ P) forms of  $\alpha$ E-cat in MDCK cells where endogenous  $\alpha$ E-cat was knocked down (Fig. 3B) (Benjamin et al., 2010). All  $\alpha$ E-cat constructs are expressed at similar protein levels that are comparable to those of endogenous  $\alpha$ E-cat in MDCK cells, where they showed a normal localization at adherens junctions (Fig. 3C)

**Fig. 1.  $\alpha$ -cat is a phosphoprotein.**

(A) Autoradiograph from SW480 cells labeled with [ $^{32}$ P]orthophosphate and affinity precipitated (ppt) or immunoprecipitated (IP) with GST, GST-ICAT or E-cad antibody. Nitrocellulose was first exposed to film ( $^{32}$ P]orthophosphate) and then subjected to western blotting (WB) with the antibodies indicated. (B) Coomassie-stained SDS gel of  $\alpha$ E-cat- $\beta$ -cat complexes captured by GST-ICAT from SW480 cells. BSA is used as a standard (Std). The  $\alpha$ -cat band of  $\sim$ 100 kDa ( $>5 \mu$ g) was excised and analyzed by collision induced dissociation (CID) MS/MS analysis (Taplin Facility, Harvard). (C) Table showing  $\alpha$ E-cat phosphopeptides identified from cells (B) or from *in vitro* kinase reaction with CK1 and CK2 (Fig. 2). Site positions are based on the neutral loss of the phosphates and fragment ions (# indicates modified residue); confident (green) and not confident (red) assignments are shown. (D) Phospho-sites cluster in a flexible region between the helical M-domain (Pokutta et al., 2002; Yang et al., 2001) and the actin-binding domain (Weiss et al., 1998). (E) Phospho-site conservation between human  $\alpha$ E-,  $\alpha$ N- and  $\alpha$ T-catenins and *Drosophila*  $\alpha$ -Cat, as well as catenins from other species. Alignment was performed using National Center for Biotechnology Information COBALT multiple-sequence alignment tool. (F,G) *En face* and *z*-stack projection immunofluorescence analysis of MDCK cell clones grown for 2 weeks on filter supports and immunostained with the antibodies indicated. Scale bar: 20  $\mu$ m.

and capacity to bind to  $\beta$ -catenin and E-cadherin (supplementary material Fig. S2G). Additional independent clones for GFP- $\alpha$ E-cat-5A and -5E are shown in supplementary material Fig. S2A.

Consistent with previous studies,  $\alpha$ E-cat silencing robustly inhibited cell-cell adhesion in an epithelial sheet mechanical dispersion assay compared with GFP- $\alpha$ E-cat-restored lines

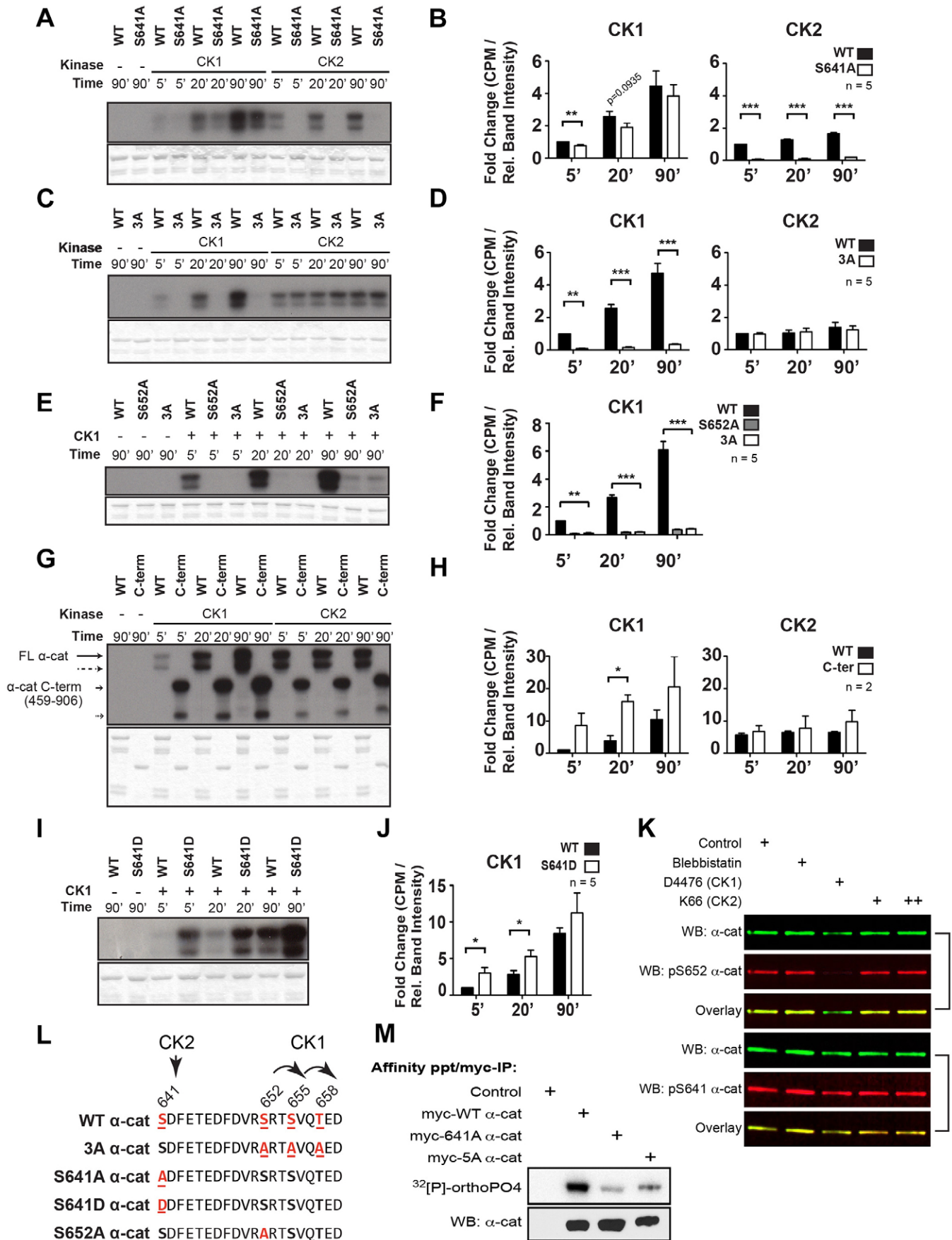


Fig. 2. See next page for legend.

**Fig. 2. Identification of major CK2 and CK1 sites in  $\alpha$ -cat.**

(A) Identification of S641 as the major CK2 site. Autoradiograph of [ $\gamma$ - $^{32}$ P]ATP *in vitro* kinase labeling of recombinant full-length (FL) and S641A (A, alanine)  $\alpha$ E-cat. The timecourse is shown in minutes ('). Coomassie-stained gel bands of purified GST-tagged  $\alpha$ E-cat proteins are shown below. WT, wild type. (B) Quantification of the data shown in A. Labeled bands were excised and quantified in a scintillation counter, and the data were plotted as a ratio of counts per minute (CPM) to relative (rel.) band intensity. (C) Identification of S652, S655 and T658 as the major CK1 sites. Autoradiograph of [ $\gamma$ - $^{32}$ P]ATP *in vitro* kinase labeling of recombinant full-length and 3A  $\alpha$ E-cat. (D) Quantification of data shown in C as above. (E) S652 is required for most [ $\gamma$ - $^{32}$ P]ATP incorporation by CK1. Autoradiograph of [ $\gamma$ - $^{32}$ P]ATP *in vitro* kinase labeling of recombinant proteins. (F) Quantification of data shown in E as above. (G) Autoradiograph of [ $\gamma$ - $^{32}$ P]ATP *in vitro* kinase labeling of recombinant full-length and the C-terminal (C-term) half of  $\alpha$ E-cat (amino acids 459–906, supplementary material Fig. S1A). The dotted arrow indicates an  $\alpha$ E-cat breakdown product that is produced during purification and that lacks C-terminal residues. (H) Quantification of data shown in G as above. (I) Phosphomimetic substitution at S641 enhances phosphorylation by CK1. Autoradiograph of [ $\gamma$ - $^{32}$ P]ATP *in vitro* kinase labeling of recombinant wild-type and S641D  $\alpha$ E-cat. (J) Quantification of the data shown in I as above. (K) Phospho-immunoblot (WB) analysis of MDCK lysates. Phosphorylation at S641 is insensitive to the CK2 inhibitor K66. Phosphorylation at S652 is sensitive to the CK1 inhibitor D4476. (L) Schematic of predicted CK2 and CK1 sites.  $\alpha$ E-cat lacking CK1 sites S652, S655 and T658 (3A  $\alpha$ E-cat), the CK2 site (S641A  $\alpha$ E-cat) or the N-terminal CK1 site (S652  $\alpha$ E-cat) are shown. (M) S641 is responsible for most  $\alpha$ E-cat phosphorylation by *in vivo* [ $^{32}$ P]orthophosphate labeling. Autoradiograph of myc-tagged  $\alpha$ E-cat proteins immunoprecipitated (by the myc tag) from transfected, [ $^{32}$ P]orthophosphate-labeled COS7 cells. After exposing hot nitrocellulose to film, it was immunoblotted with antibodies against myc (below). Data represent the mean  $\pm$  s.e.m. of at least three (B,D,H,J) or two (F) independent experiments using more than one protein preparation. \* $P$ <0.05; \*\* $P$ <0.01; \*\*\* $P$ <0.001 (Student's *t*-test).

(Fig. 3D). Epithelial sheets restored with the 5A or 641A forms of  $\alpha$ E-cat fragmented more readily upon shaking than those expressing wild-type, 5E or 641E forms of  $\alpha$ E-cat. Expression of the GFP- $\alpha$ E-cat- $\Delta$ P mutant produced an adhesion phenotype that was intermediate between phosphomimetic and non-phosphorylatable forms of  $\alpha$ E-cat. Notably, greater differences in intercellular adhesion were seen when the assay was 'sensitized' by reducing the concentration of extracellular  $\text{Ca}^{2+}$  to 0.3 and 0.1 mM. Despite these differences, cells expressing wild-type  $\alpha$ E-cat,  $\alpha$ E-cat-5A or  $\alpha$ E-cat-5E showed similar capacities to aggregate using the hanging drop assay (Thoreson et al., 2000) (supplementary material Fig. S2B–E). Taken together, these data suggest that  $\alpha$ E-cat phosphorylation contributes to the strength of cell–cell adhesion in mammalian cells, rather than to the basic capacity for cell–cell adhesion.

**P-linker mutants impair  $\alpha$ -Cat function in *Drosophila***

*Drosophila* has been used extensively to investigate the role of the CCC in tissue morphogenesis *in vivo* (Harris, 2012), and recent work has shown that *Drosophila*  $\alpha$ -Cat is essential for cadherin function (Sarpal et al., 2012). Phosphorylation of the P-linker region was detected in phosphoproteomic studies (Zhai et al., 2008). We show here that CK1 and CK2 can phosphorylate fly  $\alpha$ -Cat with similar kinetics to  $\alpha$ E-cat (Fig. 4A,B), suggesting that CK1 and CK2 consensus site phosphorylation is an evolutionarily conserved feature of  $\alpha$ -catenin proteins. To address the contribution of P-linker phosphorylation in flies, we generated several transgenic lines expressing HA-tagged mutant  $\alpha$ -Cat proteins (Fig. 4C): a mutant carrying a small deletion that removes the P-linker ( $\alpha$ Cat $\Delta$ P), two non-phosphorylatable mutants ( $\alpha$ CatT645A and  $\alpha$ CatST>A, where all 11 Ser and Thr

residues in the P-linker region were changed to Ala) and two phosphomimetic forms ( $\alpha$ CatT645D and  $\alpha$ CatST>D, a constitutively negatively charged isoform where all Ser and Thr residues in the region were changed to Asp). Multiple sequence alignment suggests that T645 in the *Drosophila* protein corresponds to S641 in  $\alpha$ E-cat (Fig. 1E). All  $\alpha$ -Cat constructs were inserted at the same genomic site to ensure similar expression levels (Fig. 4D). We have previously shown that the protein levels of a positive control  $\alpha$ Cat–HA construct inserted at the same site are comparable to those of endogenous  $\alpha$ -Cat in embryos when expressed with the Gal4-UAS system using a particular driver and temperature regime, and showed several-fold overexpression when expressed with the MARCM system in follicle cell clones of *Drosophila* egg chambers (Desai et al., 2013; Sarpal et al., 2012). Notably, strong overexpression of  $\alpha$ -Cat does not appear to have an adverse impact on normal development. Immunoblot analysis indicated that all constructs were expressed at similar protein levels in embryonic lysates (Fig. 4D). Moreover, all five mutant proteins interacted with  $\beta$ -catenin (known as Armadillo in flies), similar to  $\alpha$ Cat–HA controls (Fig. 4E), and localized to adherens junctions in embryonic epithelia (not shown) or in the follicular epithelium when expressed in wild-type cells (Fig. 4F).

To address the function of  $\alpha$ -Cat phosphorylation in *Drosophila* development, we examined the ability of our P-linker mutants to rescue  $\alpha$ -Cat mutant animals.  $\alpha$ -Cat mutants die at a late embryonic stage with severe defects in head morphogenesis (Sarpal et al., 2012). All five P-linker mutant constructs rescued embryonic head morphogenesis when expressed in  $\alpha$ -Cat mutants, similar to  $\alpha$ Cat–HA (Fig. 5A). Of the  $\alpha$ -Cat mutants expressing  $\alpha$ Cat–HA, 97% developed into adults and the remaining animals died as late pupae. By contrast, substantial levels of lethality in larval and pupal stages were observed when P-linker mutant isoforms were expressed in  $\alpha$ -Cat mutant animals so that adult survival was reduced to between 31% and 58%, dependent on the construct (Fig. 5A). Average rescue scores varied between 6.24 and 6.6 for the mutant constructs compared to 7.9 for  $\alpha$ Cat–HA. Rescue scores were determined as described previously (Desai et al., 2013). The strongest impact on survival was seen with the  $\alpha$ Cat $\Delta$ P and the  $\alpha$ CatST>D mutants. These findings show that the P-linker and its phosphorylation make an important contribution to  $\alpha$ -Cat function in *Drosophila* development. The fact that all phospho-mutants compromise  $\alpha$ -Cat function suggests not only that phosphorylation is essential, but also that de-phosphorylation of the P-linker plays a role in  $\alpha$ -Cat regulation.

The whole animal survival test described above did not provide insight into specific cellular processes that might be affected by P-linker mutations. We therefore examined the function of P-linker mutations in the follicle cells of the *Drosophila* ovary. Loss of  $\alpha$ -Cat from follicle cells that comprise the follicular epithelium surrounding the germ line cells leads to a loss of cell contacts, loss of adherens junctions and a collapse of the membrane-associated spectrin cytoskeleton (Sarpal et al., 2012). We generated positively marked  $\alpha$ -Cat mutant cell clones that expressed a P-linker mutant, or examined  $\alpha$ -Cat mutant animals that ubiquitously expressed P-linker mutants and that survived as adults. The subcellular distribution of all mutant constructs was found to be similar to that of  $\alpha$ Cat–HA or endogenous protein, when mutant isoforms are expressed in the absence of endogenous  $\alpha$ -Cat (Fig. 5C; supplementary material Fig. S3). Moreover, the distribution of DE-cadherin,  $\beta$ -catenin,  $\alpha$ -spectrin,

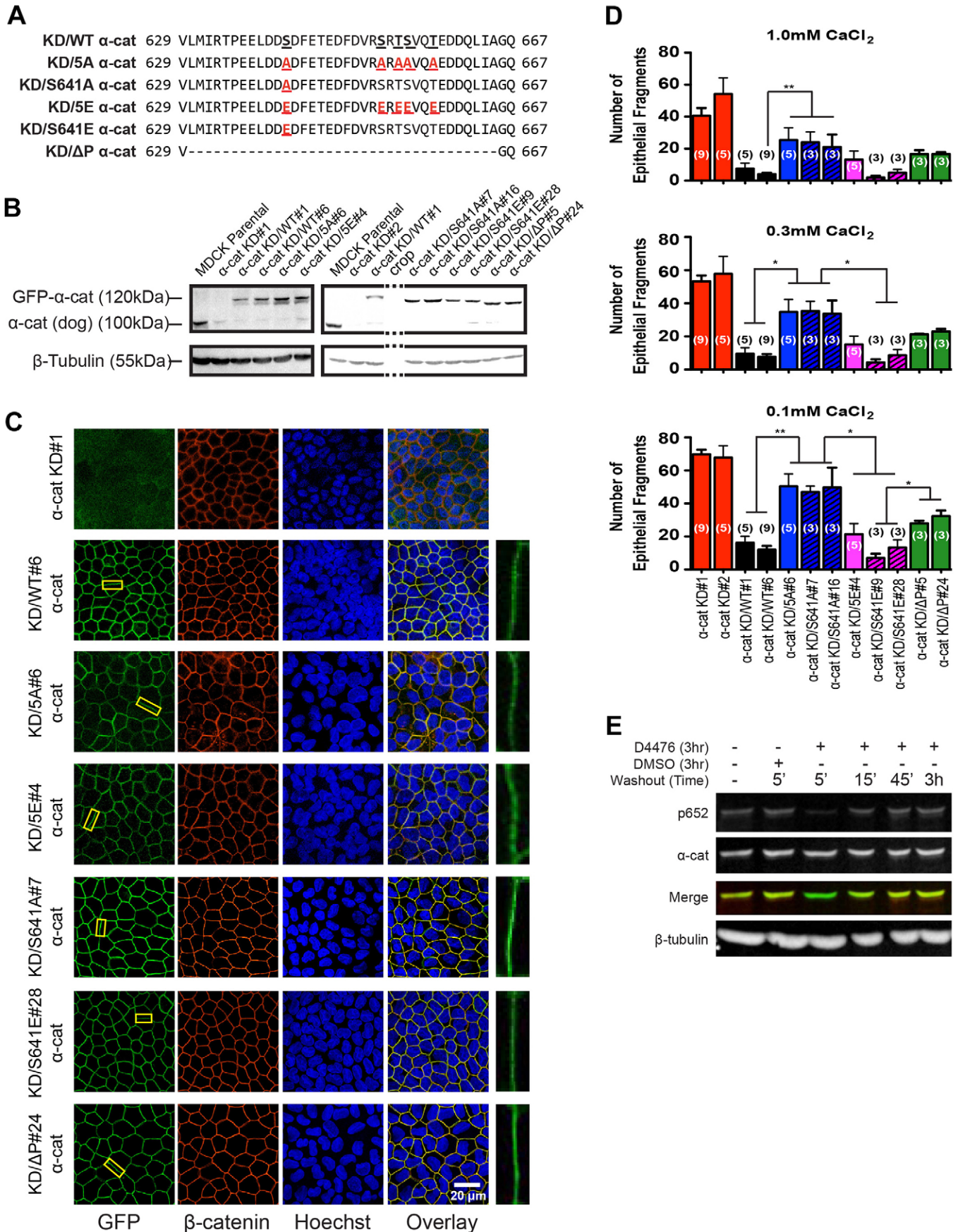


Fig. 3. See next page for legend.

**Fig. 3. The phospho-domain is required for mechanically resistant cell-cell adhesions.** (A) Schematic of P-linker mutants. KD, knockdown; WT, wild type. (B) Western blot showing MDCK knockdown/reconstitution cell clones. Independent clonal lines are shown in supplementary material Fig. S2A. (C) *En face* immunofluorescence analysis of MDCK cell clones grown for 2 weeks on filter supports. Yellow boxes indicate regions selected for higher magnification insets. Scale bar: 20  $\mu$ m. (D) Mechanical disruption assay in the presence of low (0.1 mM) to normal (1.0 mM) concentrations of  $Ca^{2+}$ . The y-axis reflects the number of macroscopic epithelial fragments counted after shaking. Data show the mean  $\pm$  s.e.m. (at least three independent experiments per cell line; *n* values are shown as white numbers within columns); \* $P < 0.05$ ; \*\* $P < 0.01$  (Student's *t*-test). Independent 5A and 5E clones are shown in supplementary material Fig. S2F. (E) Immunoblot of MDCK cell lysates incubated with the CK1 inhibitor D4476. Phosphorylation at S652 is fully inhibited after a 3-hour incubation with the inhibitor and recovers within 15 minutes after washout. Phosphorylation is inhibited by  $\sim 50\%$  after a 1-hour inhibitor treatment (C.J.G., data not shown).

and F-actin was also normal in the large majority of cells expressing P-linker mutants instead of normal  $\alpha$ -Cat (data not shown). In both  $\alpha$ -Cat mutant cell clones and whole animals, we found that the expression of P-linker mutants robustly rescued epithelial integrity in the follicular epithelium (Fig. 5B,C; supplementary material Fig. S3). For the purpose of quantification, cells were considered abnormal when they had either lost cell contact or showed an abnormal distribution of  $\alpha$ -spectrin (Sarpal et al., 2012). Rescue values tended to be lower for P-linker mutants than for  $\alpha$ Cat-HA control cells, although rescue was significantly decreased only for  $\alpha$ Cat $\Delta$ P cells. These results (Fig. 5B) are qualitatively similar to our observation in whole animal rescue experiments (Fig. 5A), and they suggest that the P-linker plays a role in follicular epithelial adhesion integrity.

We next examined border cell migration, an invasive collective migration process where border cells detach from the anterior follicular epithelium and migrate on the surface of germ line cells towards the oocyte (Montell et al., 2012). Border cells and germ line cells need to express the CCC to facilitate migration (Niewiadomska et al., 1999; Sarpal et al., 2012). Analysis of border cell migrations in  $\alpha$ -Cat mutant animals that expressed P-linker mutants showed that cells expressing  $\alpha$ Cat $\Delta$ P or  $\alpha$ CatST>D migrate significantly slower during stage 9 of oogenesis than cells expressing  $\alpha$ Cat-HA,  $\alpha$ CatT645A,  $\alpha$ CatT645D or  $\alpha$ CatST>A. Ultimately, however, migration was complete in all cases during stage 10 (Fig. 5D). Taken together, the analysis of P-linker mutations in *Drosophila* suggests that CK1 and CK2 consensus phosphorylation of  $\alpha$ -Cat makes an important contribution to CCC function.

### Negative charge substitution of $\alpha$ E-cat phospho-sites promotes more connected epithelial cell behavior during MDCK sheet migration

The reduced migration seen in *Drosophila* border cells when the P-linker is either deleted or mutated to a phosphomimetic form could result from too much or too little adhesion. To further assess the role of the P-linker in motile cells, we examined epithelial sheet migrations after scratch wounding in our GFP- $\alpha$ E-cat-restored MDCK cells (Fig. 3). We found that the wound fronts of MDCK cells with  $\alpha$ E-cat knocked down generally moved twice as fast as those of wild-type or knockdown lines where  $\alpha$ E-cat expression was restored (Fig. 6A). Of interest, cells expressing  $\alpha$ E-catS641E or  $\alpha$ E-cat5E displayed significantly faster wound-front migration rates than those expressing wild-type, 5A or 641A  $\alpha$ E-cat proteins (Fig. 6A). This faster migration is not apparently due to intrinsic

differences in cell velocities (Fig. 6B), but rather due to better persistence (Fig. 6C) and coordination or ‘connectivity’ of adjacent cells (Figs 6D–F; supplementary material Fig. S4). Identical results were observed in an independent set of GFP- $\alpha$ E-cat5A and 5E-restored MDCK clones (C.J.G., data not shown), indicating that these findings are specifically due to the  $\alpha$ E-cat mutations, and not the clonal variability of the parental MDCK cell line. Taken together, these data indicate that phosphorylation of the  $\alpha$ E-cat P-linker promotes a more coordinated epithelial cell behavior during MDCK sheet migrations.

The proximity of the P-linker region to the auto-inhibitory M3 domain, which restricts the unfurling of the M1 domain required for vinculin binding, raises the possibility that  $\alpha$ E-cat phosphorylation might destabilize the M3 domain and thereby affect  $\alpha$ -catenin binding to vinculin. This does not appear to be the case, at least for  $\alpha$ E-cat, as recombinant 5A and 5D  $\alpha$ -catenins show no difference in binding to the VinD1 domain *in vitro* or in MDCK cells by co-immunoprecipitation and colocalization analysis (Fig. 7A–F). Moreover, removing the vinculin-binding domain in the context of the  $\alpha$ E-cat5E mutant failed to affect the connectivity of cell migrations, despite reducing the physical interaction between these two proteins, indicating that vinculin recruitment to  $\alpha$ E-cat is not crucial for the improved coordination of the  $\alpha$ E-cat5E mutant in MDCK cells (Fig. 7G–L). No measureable differences in the accessibility of the mechanosensitive  $\alpha$ 18 epitope on  $\alpha$ E-cat or colocalization with the  $\alpha$ E-cat binding partner afadin were observed (supplementary material Fig. S5).

### $\alpha$ E-cat phosphorylation affects its structure locally

Our assays support the view that non-phosphorylatable and phosphomimetic forms of  $\alpha$ -catenin are functionally distinct. To determine whether phosphorylation has an impact on the structural integrity of  $\alpha$ -catenin, we subjected our recombinant  $\alpha$ E-cat mutants to trypsinolysis (Fig. 8A–E; supplementary material Fig. S5). We found that  $\alpha$ E-cat5D generates a tryptic fragment of  $\sim 30$  kDa in size that was distinct from the  $\sim 28$ -kDa fragments that were found with both the wild-type and  $\alpha$ E-cat5A proteins (Fig. 8A, compare bands 1 and 2). Edman degradation revealed that both fragments share the same N-terminal sequence, beginning at residue K384 (Fig. 8E).  $\alpha$ E-cat5D degradation revealed a novel trypsin recognition site located  $\sim 20$  amino acid residues C-terminal to the wild-type or 5A recognition site, given that  $\alpha$ E-cat5D produced a larger fragment than wild-type or  $\alpha$ E-cat5A (Fig. 8A,C). The 30-kDa fragment appeared to be converted over time to a smaller fragment that co-migrated with wild-type or  $\alpha$ E-cat5A fragments and shared the same N-terminal sequence (Fig. 8A, compare bands 2 and 3; Fig. 8E). Importantly, phosphorylation of  $\alpha$ E-cat by CK2 and CK1 generated the same tryptic pattern as seen with  $\alpha$ E-cat5D (Fig. 8B, compare bands 2 and 4). These findings suggest that phosphorylation changes the local structure of the P-linker region. No global differences between wild-type and  $\alpha$ E-cat5D were observed using circular dichroism spectra thermal denaturation analysis (Fig. 8H,I) or sizing chromatography (Fig. 8J), consistent with the view that phosphorylation affects the local conformation of the P-linker region. We also observed no reliable differences in the capacity of these  $\alpha$ E-cat proteins to associate with F-actin in solution by sedimentation analysis (Fig. 8F,G).

### DISCUSSION

Targeted knockout studies show that  $\alpha$ -catenin plays an indispensable role in cell–cell adhesion and tissue

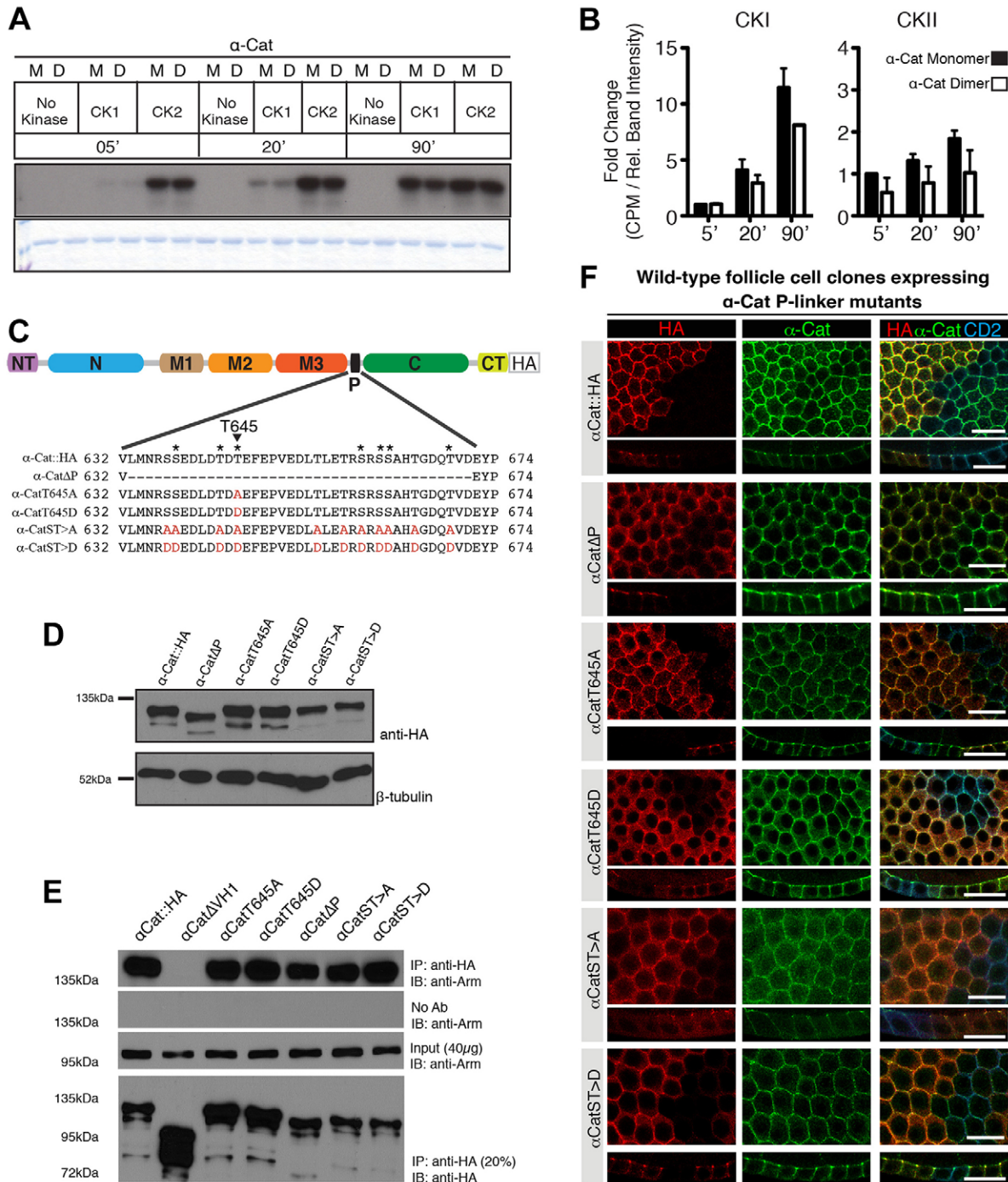


**Fig. 4. CK1 and CK2 phosphorylation of *Drosophila* αCat is not essential for β-cat/Arm binding or localization to adherens junctions.** (A) Recombinant *Drosophila* αCat was expressed in bacteria, separated into monomer ('M') and dimer ('D') fractions and phosphorylated by CK1 or CK2 in the presence of [ $\gamma$ - $^{32}$ P]ATP. The autoradiograph shows rapid phosphorylation by CK2 and comparatively slow phosphorylation by CK1. (B) The results are quantified as for Fig. 2. The data show the mean  $\pm$  s.d. (C) Schematic of αCat P-linker mutants generated for this study. Asterisks indicate Ser or Thr residues found to be phosphorylated in phosphoproteomic studies (Zhai et al., 2008). (D) HA-tagged αCat (αCat:HA) and P-linker mutants are expressed in embryos and detected in embryonic lysates using anti-HA antibodies. (E) αCat constructs immunoprecipitated (IP) from embryonic lysates with anti-HA antibody (Ab) and immunoblotted (IB) for β-catenin/Arm. (F) αCat-HA and P-linker mutants are clonally expressed in the follicular epithelium. Follicles were stained for HA to detect transgenic constructs (αCat) and CD2 to negatively mark clones. Scale bars: 10  $\mu$ m.

morphogenesis (Costa et al., 1998; Lien et al., 2006; Sarpal et al., 2012; Vasioukhin et al., 2001). However, how this multi-domain scaffold protein is regulated to mediate strong versus weak states of adhesion or other dynamic changes in adhesion is not known.

We characterized a highly conserved phospho-domain, the P-linker, in mammalian αE-cat and *Drosophila* α-Cat. Although not required for basic cell–cell adhesive function, the P-linker is nonetheless required for normal fly development, mechanically

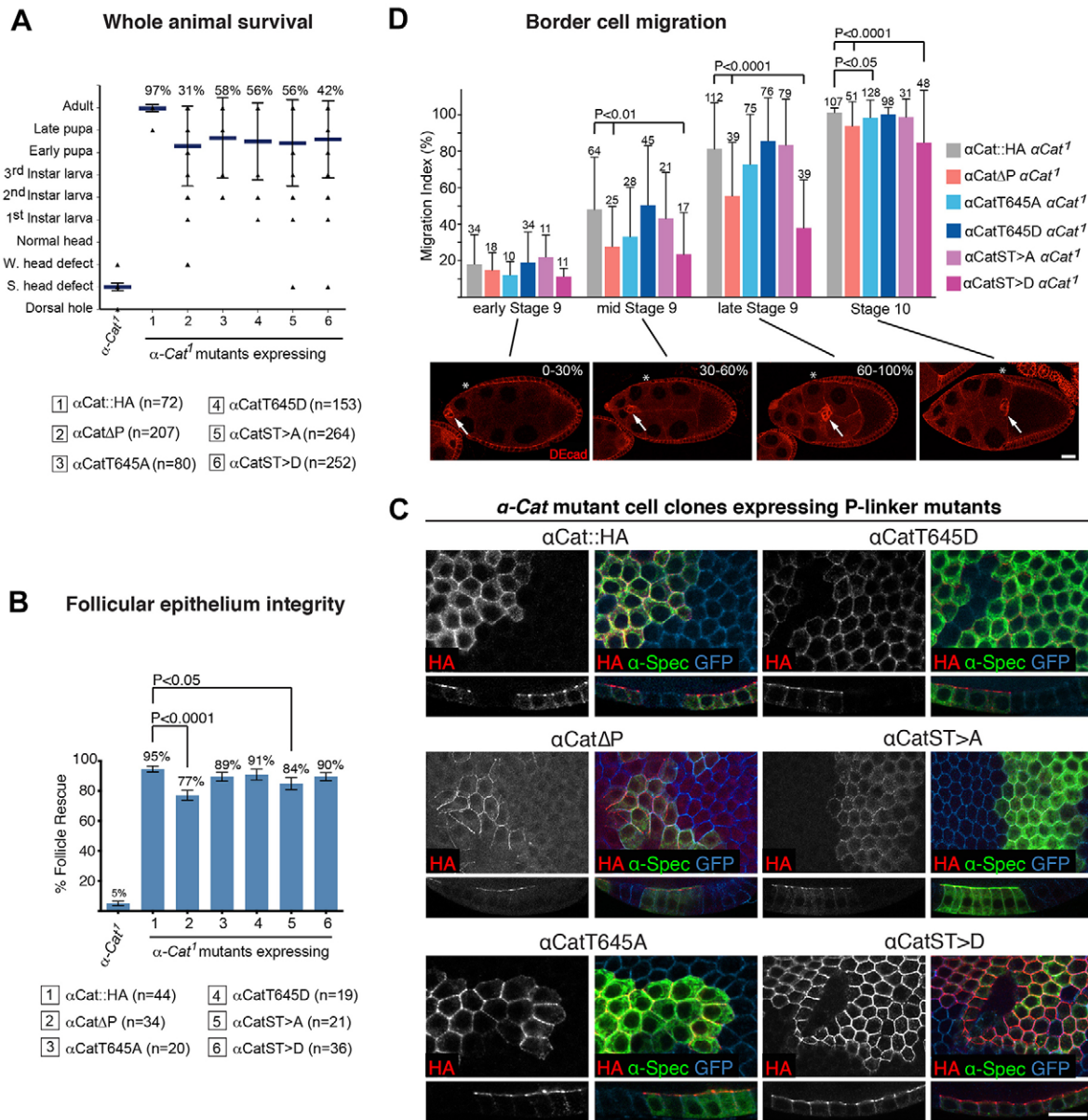


**Fig. 5. Phospho-mutants disrupt  $\alpha$ Cat function in *Drosophila*.** (A)  $\alpha$ Cat<sup>1</sup> mutant animals rescued through the ubiquitous expression of the listed  $\alpha$ Cat mutant isoforms. Animal cohorts were followed throughout development and the number of dead animals was recorded at each stage, indicated on the y-axis. If animals were embryonic lethal, we examined the cuticle to determine whether embryos showed a dorsal hole (indicating a defect in dorsal closure), a strong ('S') head defect (a failure in head involution as seen with most  $\alpha$ Cat<sup>1</sup> mutant embryos), a weak ('W') head defect (an abnormal head skeleton) or a normal head (see Sarpal et al., 2012 for a detailed description of phenotypes). Data are presented in a bar and whiskers format, showing the mean with standard deviation and the range (triangles) of phenotypes observed. Percentages above each column indicate the number of animals that survived to adulthood. The differences between the P-linker mutants and the negative and positive controls are highly significant ( $P < 0.0001$ ;  $n$  values shown in parentheses). (B, C)  $\alpha$ Cat<sup>1</sup> mutant follicle cells clones in *Drosophila* egg chambers were positively marked with GFP (using the MARCM system) and labeled for HA to detect the transgenic construct and for  $\alpha$ -Spectrin to highlight lateral membranes. Following criteria developed previously (Sarpal et al., 2012), we evaluated the integrity of cells within the follicular epithelium. (B) Data are presented as the mean  $\pm$  s.e.m. ( $n$  values given in parentheses are the number of clones evaluated, each containing many cells). All constructs showed a robust rescue of  $\alpha$ Cat<sup>1</sup> mutant cells ( $P < 0.0001$ ). The only highly significant difference to the positive control (HA-tagged  $\alpha$ Cat;  $\alpha$ Cat::HA) was seen for  $\alpha$ Cat $\Delta$ P. (C) Examples of MARCM clones showing that cells expressing P-linker mutants instead of wild-type  $\alpha$ Cat integrate normally into the follicular epithelium. All constructs enrich apically at adherens junctions. Scale bar: 10  $\mu$ m. (D) Migration of border cells in *Drosophila* egg chambers was examined in adult survivors of the whole animal rescue experiment shown in A. In wild-type animals, border cells migrate from the anterior tip of a follicle to the surface of the oocyte during stage 9 of oogenesis, and have reached the oocyte at stage 10 as shown in the panels below the graph [follicles stained for DE-cadherin (DEcad); arrow points to border cells]. Scale bar: 20  $\mu$ m. The follicular epithelium is a uniform cuboidal epithelium prior to stage 9. During stage 9 it subdivides into an anterior squamous epithelium and the posterior main body follicle cells (MBFCs). The boundary between the squamous and MBFCs is indicated by the asterisks. The distance between the anterior tip of the follicle and the surface of the oocyte was measured and set as 100%. To determine the border cell migration index we measured the distance traveled by border cells in early stage 9 (MBFC boundary 0–30%), mid stage 9 (MBFC boundary 30–60%), late stage 9 (MBFC boundary 60–100%) and stage 10. Data are presented as the mean  $\pm$  s.d. ( $n$  values are shown above each column). Significant differences in migration index between  $\alpha$ Cat $\Delta$ P and  $\alpha$ CatST>D as compared to the positive control ( $\alpha$ Cat::HA) are shown.

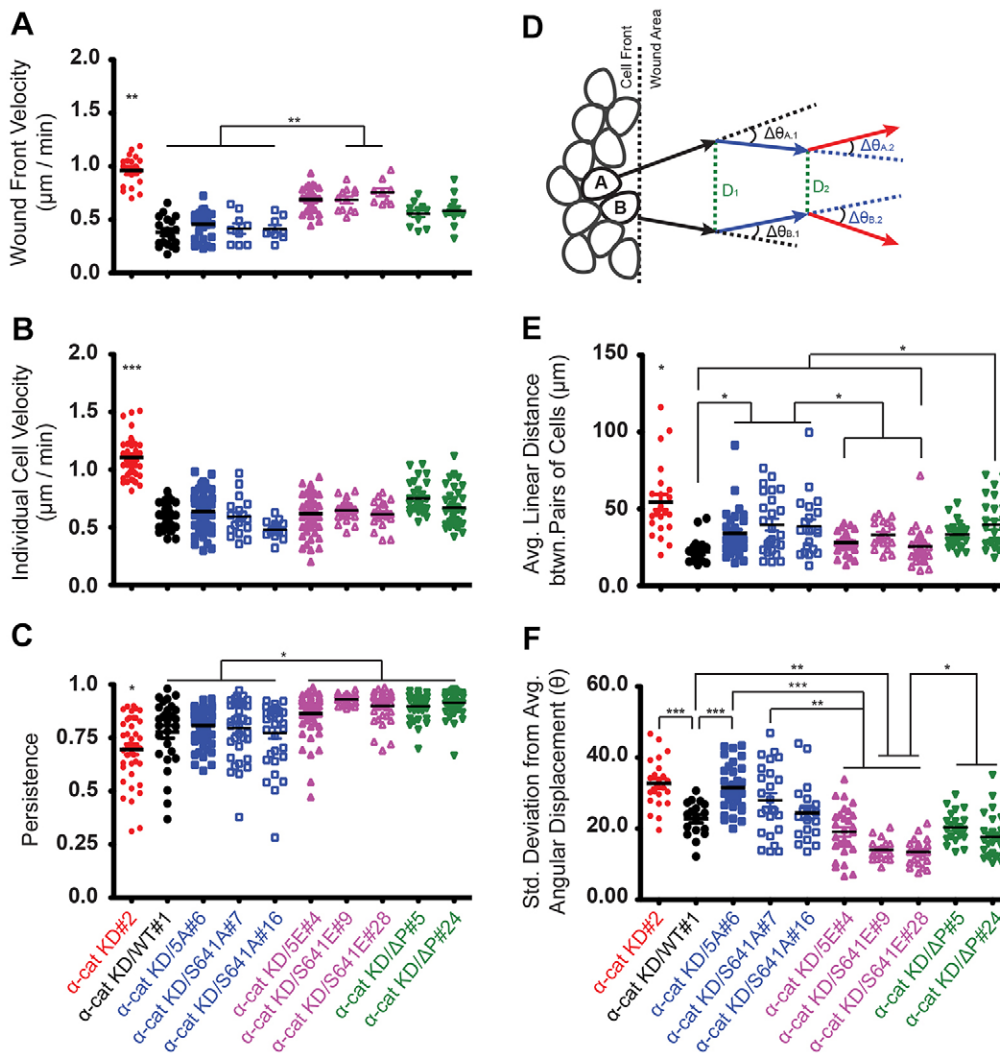


**Fig. 6. Phosphomimetic  $\alpha$ E-cat promotes faster and more connected epithelial cell behavior during MDCK sheet migrations.**

(A) Bulk wound front closure velocity. (B) Individual cell velocity measured by tracking individual cells. (C) Persistence [net cell displacement ( $\mu\text{m}$ )/total path length ( $\mu\text{m}$ )] of individual cells. (D) Schematic of the connectivity measurements performed to determine (E) average linear distance between cell pairs over the length of tracking analysis ( $\mu\text{m}$ ) and (F) standard deviation from average angular displacement over length of tracking analysis (see Methods). The data in A, B–F show the mean  $\pm$  s.e.m. from measurements made in at least ten fields of view along individual scratch wounds from two independent experiments. \* $P < 0.05$ ; \*\* $P < 0.01$ ; \*\*\* $P < 0.001$  (Student's *t*-test).

strong adhesion and efficient cell migration. As this phospho-domain lies within a flexible linker located between the mechanosensitive M-region and the C-terminal F-actin-binding domain of  $\alpha$ -catenin, our findings suggest that phosphorylation might play an important role in coordinating the activity of these domains.

Using both mass spectrometry and *in vitro* kinase assays, we showed that  $\alpha$ E-cat is phosphorylated at S641 by CK2, which appears to promote further sequential phosphorylations by CK1 at S652, S655 and T658. A similar phospho-scheme might exist for *Drosophila*  $\alpha$ Cat (T645 by CK2 and S659, S662 and T665 by CK1). Although the structural basis by which CK2 phosphorylation effectively primes  $\alpha$ -catenin for phosphorylation by CK1 is not clear, the hierarchical relationship between these phosphorylations in cells is supported by evidence that the S641A (CK2) mutant reduces the incorporation of [ $^{32}$ P]orthophosphate to the same extent as an  $\alpha$ -catenin mutant lacking all candidate phospho-sites in the region (5A mutant). Thus, the P-linker of  $\alpha$ -catenin is targeted hierarchically by distinct kinases, suggesting that this region of  $\alpha$ -catenin integrates two signals to coordinate  $\alpha$ -catenin function.

To determine the contribution of this phosphorylation scheme to  $\alpha$ -catenin function in flies and mammalian cells, we made a similar panel of mutants in both  $\alpha$ -Cat and  $\alpha$ E-cat: (1) mutants

where all Ser and/or Thr residues in the P-linker region are changed to non-phosphorylatable (Ala) or phosphomimetic (Asp or Glu) residues; (2) mutants where the hierarchically important CK2 site is changed to a non-phosphorylatable or phosphomimetic residue and (3) mutants lacking the entire P-linker region through in-frame deletion. In mammalian cells, we found that epithelial sheets restored with 5A or 641A forms of  $\alpha$ E-cat fragmented more readily upon shaking than those expressing wild-type, 5E or 641E forms of  $\alpha$ E-cat, indicating that  $\alpha$ E-cat phosphorylation promotes a more mechanically resistant cell–cell adhesion. Evidence that the negative charge status at S641 is both required and sufficient for strong cell–cell adhesion further supports the model that  $\alpha$ E-cat phosphorylation is hierarchical and crucially depends on phosphorylation at the CK2 site. Similarly, epithelial sheets restored with phosphomimetic forms of  $\alpha$ E-cat displayed faster wound closure associated with more coordinated cell–cell trajectories at the wound front compared with those expressing wild-type or non-phosphorylatable forms of  $\alpha$ E-cat. Thus, in mammalian cells, phosphorylation appears to promote the intercellular adhesive function of  $\alpha$ E-cat.

*In vivo* analysis of the function of  $\alpha$ -catenin phosphorylation in *Drosophila* suggested that the P-linker and its phosphorylation are required for normal development, as animals expressing

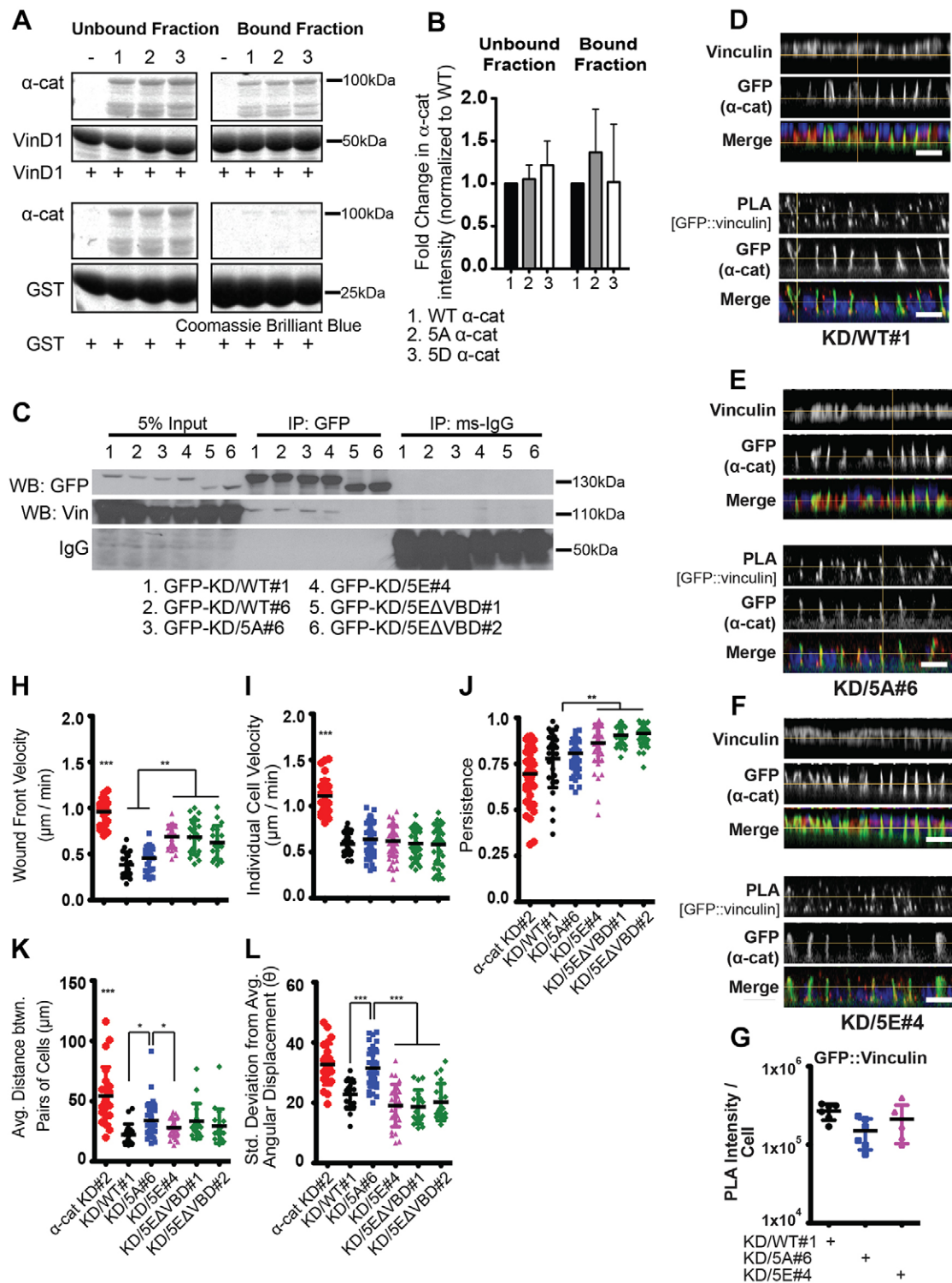


**Fig. 7. Vinculin binding to phosphomimetic  $\alpha$ E-cat is not required for enhanced connectivity.** (A) An *in vitro* binding assay demonstrates no change in  $\alpha$ E-cat–vinculin binding due to phospho-mutation or phospho-mimic. (B) Bound and unbound fractions are quantified relative to the wild-type (WT) binding condition. Data show the mean  $\pm$  s.e.m. (C) Co-immunoprecipitation (IP) analysis from MDCK cell lysates demonstrates no change in  $\alpha$ E-cat–vinculin binding due to phospho-mutation or phospho-mimic. The GFP–5E $\Delta$ VBD construct lacks the residues (277–382) required for vinculin-binding and is used as a negative control. WB, western blotting. (D–F) Cellular localization of GFP– $\alpha$ E-cat and vinculin (upper panels) and localization of the proximity ligation assay (PLA) signal between  $\alpha$ E-cat and vinculin (lower panels) along sites of cell–cell contact is shown in z-stack confocal sections in MDCK cells expressing wild-type (KD/WT#1), phospho-mutated (KD/5A#6) or phosphomimetic (KD/5E#4)  $\alpha$ E-cat. Scale bars: 20  $\mu$ m. (G) Quantification of the PLA signal observed in D–F, shown as arbitrary units per cell. No difference in PLA signal intensity due to phospho-mutated or phospho-mimetic  $\alpha$ E-cat was observed. (H–L) The faster (H,I), more persistent (J) and more coordinated (K,L) scratch-wound migration phenotype observed with phosphomimetic  $\alpha$ E-cat (KD/5E#4) does not depend on the vinculin-binding domain of  $\alpha$ E-cat. Data in G–L show the mean (black line) and range; \* $P$ <0.05; \*\* $P$ <0.01; \*\*\* $P$ <0.001 (Student's *t*-test).

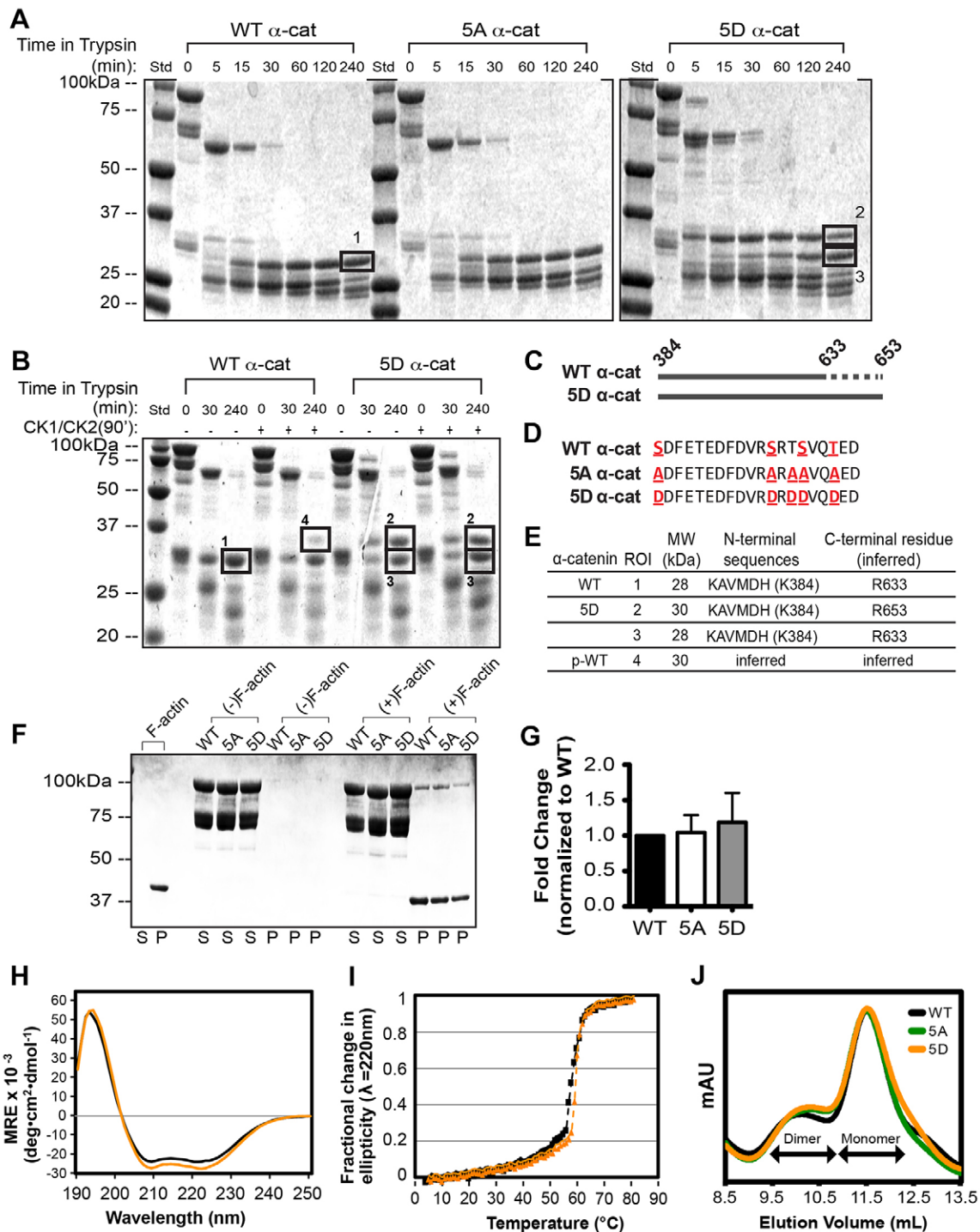


**Fig. 8. Phosphorylation at CK2 and CK1 sites affects local  $\alpha$ E-cat structure as shown by trypsinolysis.** (A) Limited proteolysis of GST affinity-purified, thrombin-cleaved wild-type (WT), 5A or 5D  $\alpha$ E-cat proteins. Coomassie-stained SDS-PAGE of proteins (14  $\mu$ M) incubated for the times indicated with 0.01 mg/ml trypsin. Std, molecular mass standard. (B) Limited proteolysis of wild-type  $\alpha$ E-cat after *in vitro* phosphorylation by CK2 and CK1 compared to that of 5D  $\alpha$ E-cat. (C,D) Schematics of inferred trypsin digestion sites for wild-type and 5D  $\alpha$ E-cat proteins. (E) N-terminal sequence identification from regions of interest (ROIs) by MS/MS and Edman degradation performed on a repeat experiment shown in supplementary material Fig. S5J. (F) Sedimentation of GST affinity-purified, thrombin-cleaved wild-type, 5A and 5D  $\alpha$ E-cat proteins, in the presence or absence of F-actin. Supernatant ('S') and pellet ('P') fractions were analyzed by SDS-PAGE and Coomassie staining. (G) Quantification of the data shown in F. Densitometry was performed on  $\alpha$ E-cat bands in the pellet fraction, and data were normalized to actin loading and expressed as the fold change in binding with respect to the wild-type binding condition. Data show the mean  $\pm$  s.e.m. (H) Circular dichroism spectra of wild-type (black) and 5D (yellow)  $\alpha$ E-cat. MRE, mean residue ellipticity. (I) Thermal unfolding of wild-type (black) and 5D (yellow)  $\alpha$ E-cat proteins. (J) Size-exclusion chromatography (SEC) of GST-affinity purified, thrombin-cleaved wild-type, 5A or 5D  $\alpha$ E-cat proteins, collected on a Superdex-200 analytical column. mAU, milli-absorption units. Proteins used for trypsinolysis and F-actin co-sedimentation were not previously separated by SEC, but were diluted from similarly concentrated ( $\sim$ 30  $\mu$ M) stock solutions and thus expected to contain comparable equilibrium mixtures of monomers and dimers.

P-linker mutants instead of endogenous  $\alpha$ -Cat showed reduced viability. Although non-phosphorylatable and phosphomimetic versions of  $\alpha$ -Cat supported the integrity of the follicular epithelium and restored embryonic head morphogenesis, each could inhibit development through larval and pupal stages, indicating that both kinds of mutations compromise normal  $\alpha$ -Cat function. In contrast to whole animal survival and the follicular epithelium, analysis of border cell migration revealed that non-phosphorylatable and phosphomimetic versions of  $\alpha$ -Cat are functionally distinct, as border cells in flies expressing  $\alpha$ CatST>D instead of  $\alpha$ -Cat migrated significantly slower than wild-type or  $\alpha$ Cat-HA- and  $\alpha$ CatST>A-expressing flies. As border cell migration speed is sensitive to both elevated and reduced cadherin-based adhesion (Niewiadowska et al., 1999; Schober et al., 2005), it is difficult to infer from this analysis whether  $\alpha$ -Cat phosphorylation enhances or weakens adhesion. However, given that the equivalent mutation in  $\alpha$ E-cat ( $\alpha$ Ecat5E) is associated with stronger cell–cell adhesion, we reason that  $\alpha$ CatST>D slowed border cell migration by enhancing cadherin-based adhesion. These data also suggest that cycles of  $\alpha$ -catenin phosphorylation and dephosphorylation are likely to be required for normal function. Indeed, short-term CK1 inhibition blocked  $\alpha$ E-cat phosphorylation at S652, whereas phosphorylation is fully restored within 5–15 minutes after wash out (Fig. 3E), suggesting that  $\alpha$ -catenin phosphorylation is poised for dephosphorylation.

Although the mechanism by which phosphomimetic forms of  $\alpha$ -catenin enhance cell–cell adhesion is not clear, a recent study by the Troyanovsky group found that the flexible P-linker region between the M- and actin-binding domains, in the context of an E-cadherin– $\alpha$ E-cat chimera, was important for cadherin cluster stability and adherens junction formation (Hong et al., 2013), raising the possibility that phosphorylation within the P-linker might impact on the relative stiffness and thereby coordination of F-actin binding and mechanosensitive M-domains in  $\alpha$ -catenin. Although we found no consistent difference in the activity of DE-cadherin– $\alpha$ -Cat fusion proteins in *Drosophila*, where only the actin-binding domain of  $\alpha$ -Cat was fused to DE-cadherin either with or without the P-linker region (U.T., data not shown), trypsinolysis of phosphorylated or phosphomimetic  $\alpha$ E-cat recombinant proteins promoted the stabilization of a new tryptic polypeptide that appears to have resulted from altered intramolecular interactions involving the P-linker, demonstrating that phosphorylation can alter the local conformation of  $\alpha$ E-cat. Although such a structural change does not apparently affect  $\alpha$ E-cat binding to F-actin in solution, it might be more important when actin filaments are under tension, contributing to the recently described catch-bond behavior of the  $\alpha$ E-cat–F-actin interaction (Buckley et al., 2014). Lastly, charge status of the P-linker region did not obviously affect  $\alpha$ -catenin binding to vinculin, and the latter was not responsible for the improved connectivity of migrating cells. Whether  $\alpha$ -catenin phosphorylation affects binding to other proteins known to interact with the M-domain is not known.

The kinases and upstream signals that regulate  $\alpha$ -catenin are only partly understood. Although  $\alpha$ E-catS641 is the major CK2 phosphorylation site *in vitro*, pharmacologic inhibition of CK2 failed to inhibit phosphorylation at this site in cells, indicating that the priming kinase for  $\alpha$ E-cat either is not CK2 or is redundantly regulated by other kinases. Pharmacologic inhibition of CK1 blocked phosphorylation at  $\alpha$ E-catS652, as well as bulk [ $^{32}$ P]orthophosphate incorporation (Dupre-Crochet et al., 2007), suggesting that  $\alpha$ -catenin phosphorylation in cells might be

carried out predominantly by a CK1 family member. In this regard, an siRNA screen targeting signaling regulators of epithelial sheet migration in MCF10A breast epithelial cells identified CK1 $\epsilon$  and  $\gamma$ 2 as required for normal migrations, where their loss led to reduced cell–cell adhesion and erratic migration (Simpson et al., 2008). Although CK1 $\epsilon$  and  $\gamma$ 2 no doubt phosphorylate many proteins that contribute to sheet migrations,  $\alpha$ E-cat is a reasonably abundant structural protein and thus might be a key target driving the CK1 $\epsilon$  and  $\gamma$ 2 loss-of-function phenotype. Understanding the upstream signals that regulate CK1 accessibility and activity towards  $\alpha$ -catenin will be the subject of future investigation.

In addition to  $\alpha$ -catenin, other components of the CCC are highly phosphorylated (Stappert and Kemler, 1994), but the identification of key sites and their relative contribution to the regulation of cell–cell adhesion is only just emerging. Three serine residues within the  $\beta$ -catenin binding domain of E-cadherin are responsible for most  $^{32}$ P labeling,  $\beta$ -catenin binding and the mutual stabilization of  $\beta$ -catenin and E-cadherin at the cell surface (McEwen et al., 2014). Whereas E-cadherin serine phosphorylation appears to be largely constitutive in cell cultures, transient inhibition during tissue development would be predicted to have consequences for adhesion-dependent processes. Conversely, phosphorylation of  $\beta$ -catenin on Y654 can reduce its affinity for E-cadherin (Roura et al., 1999; Tamada et al., 2012; van Veelen et al., 2011), and conditional knock-in mice reconstituted with a phosphomimetic form of  $\beta$ -catenin die during embryogenesis (van Veelen et al., 2011). Thus, whereas point mutations that inhibit phosphorylation in  $\alpha$ -catenin (this study) or  $\beta$ -catenin (Tamada et al., 2012; van Veelen et al., 2011) generally do not interfere with basic CCC formation and epithelial integrity, normal development is nonetheless compromised, emphasizing the essential role of catenin phosphoregulation for tissue morphogenesis. Given the number of disease states where cell–cell adhesive function is perturbed without evidence of strong loss-of-function mutations in the CCC [e.g. asthma (Xiao et al., 2013), inflammatory bowel disease (Thompson and Lees, 2011) and vascular edema (Weis et al., 2004)], understanding how CCC phosphorylation regulates strong versus weak adhesion might inform strategies to reinforce CCC function when necessary.

## MATERIALS AND METHODS

### Phosphopeptide mapping

SW480 colon carcinoma cells were obtained from American Type Culture Collection (Manassas, VA) and maintained in DMEM with 10% FBS and penicillin-streptomycin. Cells were lysed in standard 1% Triton X-100 lysis buffer (20 mM Tris-HCl pH 7.5, 1% Triton X-100, 150 mM NaCl, 5 mM EDTA, 10% glycerol) containing protease inhibitors (Roche, Basel, Switzerland). Endogenous  $\alpha$ E-catenin was precipitated from SW480 cell lysates using GST-ICAT as described previously (Maher et al., 2010). Precipitated proteins were visualized with SDS-PAGE and Coomassie staining. The 100-kDa band was excised, digested with trypsin and analyzed by high mass accuracy electrospray tandem mass spectrometry (LC-MS/MS) and nano-electrospray tandem mass spectrometry at the Taplin Biological Mass Spectrometry Facility (Harvard Medical School, Boston, MA). MS/MS spectra were searched using the Sequest algorithm and phosphopeptides were assigned based on several scores including mass accuracy (Beausoleil et al., 2004).  $\alpha$ E-catenin protein coverage by amino acid was 836/906 (92.3%); coverage by mass was 91737/100072 (91.7%) with 115 matches. Validation of recombinant  $\alpha$ E-catenin *in vitro* phosphorylation by CK1 by mass spectrometric analysis (Northwestern University; Chemistry of Life Sciences, Chicago, IL) using the phosphoRS algorithm showed that

peptide sRtSVQfEDDQLIAGQSAR is multi-phosphorylated at S1, T3 and T7 positions. Manually verified sites showed three neutral losses of phosphoric acid and their corresponding precursor ion mass [1102.08 D (1P), 1054.15(2P), 1005.23 (3P)], confirming multi-phosphorylation. Precursor ion analysis of the collision induced dissociation (CID) spectrum revealed that phosphorylation at T3 is not highly confident and S4 might be modified instead.

### Antibodies and $\alpha$ E-catenin mutants

The following antibodies were used in this study: rabbit anti-GFP (A11122, Invitrogen), mouse monoclonal anti- $\alpha$ -cat 5B11 (Daugherty et al., 2014), mouse monoclonal anti- $\alpha$ -catenin (610193, BD Biosciences), rabbit polyclonal anti-phospho-Ser641- $\alpha$ E-catenin (21330, Signalway, College Park, MD) and rabbit polyclonal anti-phospho-Ser652- $\alpha$ E-catenin (13061, Cell Signaling Technology, Danvers, MA). Human and murine  $\alpha$ E-catenin site-specific point mutants were generated using the Stratagene QuikChange II Site-Directed Mutagenesis kit and QuikChange Primer Design Program. Primers used for human and mouse phospho-mutants are available upon request. The P-linker ( $\Delta$ P) mutant removed amino acids 630–666, joining V629 to Q667 using the Clontech In Fusion<sup>®</sup> HD Cloning kit (Clontech, Mountain View, CA). The dog  $\alpha$ E-catenin KD/GFP:: $\alpha$ E-catenin vector (pBG14) was kindly provided by the James Nelson laboratory (Stanford, CA).

### Cell culture and stable cell line selection

MDCK and SW480 cells were obtained from American Type Culture Collection (ATCC, Manassas, VA) and maintained in Dulbecco's Modified Eagle's Medium [DMEM, Corning, (Corning, NY)], containing 10% fetal bovine serum [FBS, Atlanta Biologicals (Flowery Branch, GA) or JRS Scientific (Woodland, CA)], 100 U/ml penicillin and 100  $\mu$ g/ml streptomycin (Corning). Stable KD/GFP- $\alpha$ E-catenin MDCK cell clones were selected with 0.8 mg/ml G418 sulfate (Corning), ring-cloned and sorted to homogeneity for GFP fluorescence by flow cytometry using a MoFlo Legacy (BD Biosciences, San Jose, CA) or FacsAria5 (BD Biosciences).

### Epithelial sheet mechanical dispersion assay

MDCK KD/GFP- $\alpha$ E-catenin clones were subjected to a mechanical dispersion assay using the neutral protease dispase (Roche) (McEwen et al., 2014). The upper limit for counting was 75 epithelial fragments.

### Immunofluorescence, proximity ligation assay and imaging

MDCK KD/GFP- $\alpha$ E-cat clones were grown on high-pore-density filter supports (Corning) and fixed in ice-cold methanol for 10 minutes. Immunofluorescence was carried out using standard procedures with the indicated antibodies. Colocalization analysis using proximity ligation secondary antibodies was carried out using the manufacturer's recommendations (Olink Biosciences, Stockholm, Sweden) with species-matched IgG controls. Images were captured using a Nikon AIR+ confocal microscope (Nikon, Tokyo, Japan) equipped with 40 $\times$  Plan Fluor NA1.4 and 60 $\times$  Plan Apo NA1.45 objectives and galvano scanner under the control of the NIS-Elements AR software. Images were processed using Adobe Photoshop<sup>®</sup> (Adobe, San Jose, CA) and ImageJ software.

### Scratch wound assay

MDCK cells were plated on MatTek 35-mm glass-bottomed culture dishes (P35G-1.0-14-C, VWR, Radnor, PA) at a seeding density of  $1.0 \times 10^6$  cells. After 16 hours, the monolayer was washed in DMEM+10% FBS. At 24 hours post-plating, a wound was made using a Neptune BT10XL or BT1250 pipette tip (VWR). After 2 hours of recovery, the monolayer was washed three times in DMEM+10% FBS to remove cell debris at the wound front. Cells were imaged at 20 $\times$  magnification every 10 minutes for 12–14 hours at 37 $^{\circ}$ C on a Nikon Biostation IM-Q. Ten fields of view were imaged along the wound edge. Wound healing analysis was quantified as described below using the MTrackJ plugin on ImageJ.

### Tracking analysis

Individual cells at the wound front were followed using the MTrackJ plugin in ImageJ software. Bulk wound front velocity was measured as the rate ( $\mu$ m/min) of wound front migration. Individual cell velocity ( $\mu$ m/min) was calculated by averaging the distance ( $\mu$ m) traveled by each cell per frame (10 minutes). Persistence was calculated by dividing the net linear displacement ( $\mu$ m) of each cell by the total distance traveled ( $\mu$ m). The mean distance ( $D$ ) between the nuclei of pairs of neighboring cells was calculated over each frame. Connectivity was measured as the sample standard deviation of the mean angular displacement for each pair of cells according to the formula below, where in every frame ( $N$ ) the angular displacement from the previous frame ( $\Delta\theta$ ) was obtained for each cell (A and B), then averaged between the cells, and the sample standard deviation from this mean was measured. Sample standard deviation of average angular displacement =

$$\sqrt{\frac{1}{N-1} \sum_{i=1}^N \left[ (\Delta\theta_{AorB}) - \left( \frac{|\Delta\theta_A| + |\Delta\theta_B|}{2} \right)_i \right]^2}$$

### $\alpha$ E-catenin protein purification and characterization

Glutathione-S-transferase (GST)-tagged  $\alpha$ E-catenin proteins (pGEX-4T) were expressed in BL21 (DE3) Codon Plus *Escherichia coli*, solubilized (1% Triton X-100, 50 mM Tris, 5 mM EDTA, 150 mM NaCl, 0.1 mM DTT), sonicated, isolated using glutathione-Sepharose 4B beads (GE Healthcare) and either eluted using 300 mM L-glutathione or cleaved using bovine thrombin (Sigma). Proteins were dialyzed into storage buffer (15 mM Tris, 5 mM MgCl<sub>2</sub>, 300 mM NaCl, 0.1 mM DTT, 10% sucrose), flash-frozen and stored at  $-80^{\circ}$ C. Trypsinolysis was performed as described previously (Drees et al., 2005). N-terminal Edman sequencing of protein samples blotted onto PVDF membrane was performed at the SPARC BioCentre (Hospital For Sick Children, Toronto, Ontario, Canada). Circular dichroism spectroscopic data for 20–30  $\mu$ M  $\alpha$ E-catenin samples were collected on a Jasco J-815 CD spectrometer (Jasco, Tokyo, Japan) using a 0.01-cm path length cuvette with a scanning speed of 20 nm/min (1 nm increments). Thermal melt data were acquired at a scan rate of 1 $^{\circ}$ C/min. Dimer and monomer fractions were separated by size-exclusion chromatography using a Superdex-200 analytical column. *In vitro* kinase assays were performed at 30 $^{\circ}$ C with 100 units of casein kinase 1 or 2 (New England Biolabs, Ipswich, MA) at a protein concentration of 2–4  $\mu$ M in 200  $\mu$ M ATP, 0.04  $\mu$ Ci/ $\mu$ l [ $\gamma$ -<sup>32</sup>P]ATP (Perkin Elmer, Waltham, MA). Densitometry of Coomassie-stained bands was carried out using ImageJ. Radioactivity was quantified in Bio-Safe NA scintillation cocktail (RPI Corp., Mt Prospect, IL) using a Beckman LS 6500 scintillation counter.

### F-actin co-sedimentation assay

F-actin was prepared according to the instructions of the kit manufacturer (Cytoskeleton Inc., Denver, CO). Actin and  $\alpha$ E-cat recombinant proteins were incubated in F-buffer at a final concentration of 10  $\mu$ M for 1 hour at room temperature. Samples were centrifuged at 100,000  $g$  for 30 minutes at 20 $^{\circ}$ C. Supernatant and pellet fractions were analyzed by SDS-PAGE. Densitometry of Coomassie-stained bands was carried out using ImageJ.

### Generation of *Drosophila* phospho-mutants and transgenes

PCR-mediated site-directed mutagenesis was used to generate transgenic constructs: *UAS-aCatAP*, *UAS-aCatT645A*, *UAS-aCatT645D*, *UAS-aCatST>A*, and *UAS-aCatST>D*. Primers can be provided on request. Mutagenesis was carried out using the vector *pBSACAT* containing the coding sequence for *a-Cat*, except that its stop codon was replaced with a *NotI* restriction site. Mutated *a-Cat* cDNAs were excised from *pBSACAT* using *NotI* and cloned into the *pUASP-attB* transformation vector containing a C-terminal 2X-HA epitope tag. Transgenic flies were produced by Genetic Services Inc. (Cambridge, MA). All HA-tagged constructs were inserted into the *attP2* recombination target site on the third chromosome (Groth et al., 2004).

### **Drosophila genetics**

*hs-Flp, Act>CD2>Gal4* (Pignoni et al., 1997) was used to clonally express recombinant lines in the follicular epithelium. MARCM analysis was carried out as described previously (Desai et al., 2013; Lee and Luo, 1999; Sarpal et al., 2012). Overexpression analysis and rescue experiments (in embryos and ovaries) were performed as described previously (Desai et al., 2013). Briefly, to quantify whole animal rescue experiments and to establish a rescue score, we selected cohorts of embryos of the appropriate genotype and followed them through development. The cuticle of lethal embryos was examined and scored as –1 (dorsal hole), 0 (strong head defect – this defect is seen in most *a-Cat* zygotic-null mutants), 1 (weak head defect) and 2 (no defect). Additional scores correspond to lethal phase: 3 (1st larval instar), 4 (2<sup>nd</sup> larval instar), 5 (3<sup>rd</sup> larval instar), 6 (early pupa), 7 (late pupa) and 8 (adult) (Sarpal et al., 2012; Desai et al., 2013). The following recombinant lines were used for embryonic rescue experiments: (1) *act-Gal4 da-Gal4 a-Cat<sup>1</sup>/TM3-Ser, twi-Gal4, UAS-GFP* (Sarpal et al., 2012); (2) *UAS-aCatΔP a-Cat<sup>1</sup>/TM3-Ser, twi-Gal4, UAS-GFP*; (3) *UAS-aCatT645A a-Cat<sup>1</sup>/TM3-Ser, twi-Gal4, UAS-GFP*; (4) *UAS-aCatT645D a-Cat<sup>1</sup>/TM3-Ser, twi-Gal4, UAS-GFP*; (5) *UAS-aCatST>A a-Cat<sup>1</sup>/TM3-Ser, twi-Gal4, UAS-GFP*; (6) *UAS-aCatST>D a-Cat<sup>1</sup>/TM3-Ser, twi-Gal4, UAS-GFP*.

The following recombinant lines were used for MARCM analysis: (1) *hs-Flp, FRT40A; da-Gal4, UAS-mCD8::GFP, a-Cat<sup>1</sup>/TM6b* (Sarpal et al., 2012); (2) *tub-Gal80, ubi-a-Cat, FRT40A; act-Gal4, UAS-aCatΔP, a-Cat<sup>1</sup>/TM6b*; (3) *tub-Gal80, ubi-a-Cat, FRT40A; act-Gal4, UAS-aCatT645A, a-Cat<sup>1</sup>/TM6b*; (4) *tub-Gal80, ubi-a-Cat, FRT40A; act-Gal4, UAS-aCatT645D, a-Cat<sup>1</sup>/TM6b*; (5) *tub-Gal80, ubi-a-Cat, FRT40A; act-Gal4, UAS-aCatST>A, a-Cat<sup>1</sup>/TM6b*; (6) *tub-Gal80, ubi-a-Cat, FRT40A; act-Gal4, UAS-aCatST>D, a-Cat<sup>1</sup>/TM6b*.

### **Drosophila immunocytochemistry**

Ovaries were fixed in 5% formaldehyde in phosphate buffer for 13 minutes. The primary antibodies used were: anti-HA (rat monoclonal 3F10, 1:600; Roche), anti- $\alpha$ -spectrin [mouse monoclonal, 1:20; Developmental Studies Hybridoma Bank (DSHB, University of Iowa, Iowa City, IA)]; anti-CD2 [mouse polyclonal, 1:250, Serotec (Raleigh, NC)], anti- $\alpha$ Cat (guinea pig polyclonal GP121, 1:1000, Sarpal et al., 2012), anti-GFP (mouse monoclonal JL-8, 1:400, Clontech) and anti-GFP–Alexa-Fluor-488 (mouse polyclonal, 1:500, Invitrogen).

### **Measurement of the border cell migration index**

Border cell migration index was calculated as described previously (Gunawan et al., 2013; Melani et al., 2008). Border cells migrate from the anterior tip of the follicle (0% migration) to the nurse-cell–oocyte boundary (100% migration) during stage 9 of oogenesis. We subdivided stage-9 follicles into three phases based on the position of the boundary between anterior squamous follicle cells and the posterior columnar follicle cells, which are also referred to as main body follicle cells (MBFC boundary): early stage 9 (MBFC boundary, 0–30%), mid stage 9 (MBFC boundary; 30–60%) and late stage 9 (MBFC boundary; 60–100%). We determined the distance traveled by the border cell cluster for each phase of stage 9 and for stage 10 follicles. The migration index was calculated as the distance traveled by the border cells relative to the distance between the anterior tip of the egg chamber and the oocyte–nurse-cell boundary. Prism6 (GraphPad Software) was used for statistical analysis (unpaired, two-tailed Student's *t*-test).

### **Drosophila immunoblotting and immunoprecipitation**

Immunoblots and immunoprecipitation experiments were conducted as described previously (Desai et al., 2013). The following primary antibodies were used: anti-HA (rat polyclonal 3F10, 1:1000; Roche), anti-Arm (mouse monoclonal N74A1, 1:1000; DSHB) and anti- $\beta$ -tubulin (mouse monoclonal E7, 1:1000, DSHB). Horseradish peroxidase (HRP)-coupled secondary antibodies (Jackson Immunoresearch Laboratories) were used at a dilution of 1:1000.

### **Drosophila image acquisition, quantification and statistical analysis**

Fixed embryos and ovaries were imaged on either a LSM510 (Carl Zeiss Inc.) or a SP5 confocal microscope at room temperature using a 40 $\times$  objective lens. Captured images were processed in Adobe Photoshop and Adobe Illustrator (Adobe). Quantification of rescue experiments in embryos and ovaries was performed as described previously (Desai et al., 2013).

### **Acknowledgements**

We thank Sarah Rice's laboratory for protein purification support and use of their FPLC, and members of the Tepass and Gottardi laboratories for critically reading the manuscript.

### **Competing interests**

The authors declare no competing or financial interests.

### **Author contributions**

D.J.E., R.D., N.I., S.S.F., M.N.N., A.S.F., D.N., R.L.D., R.M. and R.S. carried out experiments. D.L. provided advice. N.I., M.I., U.T. and C.J.G. designed experiments and wrote the manuscript.

### **Funding**

Northwestern University (NU) Flow Cytometry and Center for Advanced Microscopy are supported by the Robert H. Lurie Comprehensive Cancer Center Support Grants [grant numbers NCI CA060553 and P30 CA060553, respectively]; with support from the NU Skin Disease Research Center. U.T. is supported by the Canadian Cancer Society Research Institute [grant number 020431]; and M.I. and U.T. are supported by the Canadian Institutes for Health Research [grant numbers 130297 and IG1-94507]. D.L. and M.N.N. are funded by the National Science Foundation [grant numbers 11-32116 and DGE-1324585]. The Gottardi laboratory is supported by the National Institutes of Health [grant numbers F31 GM101959 to D.J.E., T32CA09560 to S.S.F. and GM076561 to C.J.G.]. Deposited in PMC for release after 12 months.

### **Supplementary material**

Supplementary material available online at <http://jcs.biologists.org/lookup/suppl/doi:10.1242/jcs.163824/-DC1>

### **References**

- Ballif, B. A., Villén, J., Beausoleil, S. A., Schwartz, D. and Gygi, S. P. (2004). Phosphoproteomic analysis of the developing mouse brain. *Mol. Cell. Proteomics* **3**, 1093–1101.
- Barry, A. K., Tabdili, H., Muhamed, I., Wu, J., Shashikanth, N., Gomez, G. A., Yap, A. S., Gottardi, C. J., de Rooij, J., Wang, N. et al. (2014).  $\alpha$ -catenin cytomechanics – role in cadherin-dependent adhesion and mechanotransduction. *J. Cell Sci.* **127**, 1779–1791.
- Bauer, A., Lickert, H., Kemler, R. and Stappert, J. (1998). Modification of the E-cadherin-catenin complex in mitotic Madin-Darby canine kidney epithelial cells. *J. Biol. Chem.* **273**, 28314–28321.
- Beausoleil, S. A., Jedrychowski, M., Schwartz, D., Elias, J. E., Villén, J., Li, J., Cohn, M. A., Cantley, L. C. and Gygi, S. P. (2004). Large-scale characterization of HeLa cell nuclear phosphoproteins. *Proc. Natl. Acad. Sci. USA* **101**, 12130–12135.
- Benjamin, J. M., Kwiatkowski, A. V., Yang, C., Korobova, F., Pokutta, S., Svitkina, T., Weis, W. I. and Nelson, W. J. (2010). AlphaE-catenin regulates actin dynamics independently of cadherin-mediated cell-cell adhesion. *J. Cell Biol.* **189**, 339–352.
- Buckley, C. D., Tan, J., Anderson, K. L., Hanein, D., Volkman, N., Weis, W. I., Nelson, W. J. and Dunn, A. R. (2014). Cell adhesion. The minimal cadherin-catenin complex binds to actin filaments under force. *Science* **346**, 1254211.
- Burks, J. and Agazie, Y. M. (2006). Modulation of alpha-catenin Tyr phosphorylation by SHP2 positively effects cell transformation induced by the constitutively active FGFR3. *Oncogene* **25**, 7166–7179.
- Chen, J., Lu, Y., Meng, S., Han, M. H., Lin, C. and Wang, X. (2009). alpha- and gamma-Protocadherins negatively regulate PYK2. *J. Biol. Chem.* **284**, 2880–2890.
- Choi, H. J., Pokutta, S., Cadwell, G. W., Bobkov, A. A., Bankston, L. A., Liddington, R. C. and Weis, W. I. (2012).  $\alpha$ E-catenin is an autoinhibited molecule that coactivates vinculin. *Proc. Natl. Acad. Sci. USA* **109**, 8576–8581.
- Costa, M., Raich, W., Agbunag, C., Leung, B., Hardin, J. and Priess, J. R. (1998). A putative catenin-cadherin system mediates morphogenesis of the *Caenorhabditis elegans* embryo. *J. Cell Biol.* **141**, 297–308.
- Daugherty, R. L., Serebryanny, L., Yemelyanov, A., Flozak, A. S., Yu, H. J., Kosak, S. T., deLanerolle, P. and Gottardi, C. J. (2014).  $\alpha$ -Catenin is an inhibitor of transcription. *Proc. Natl. Acad. Sci. USA* **111**, 5260–5265.

- Dephoure, N., Zhou, C., Villén, J., Beausoleil, S. A., Bakalarski, C. E., Elledge, S. J. and Gygi, S. P. (2008). A quantitative atlas of mitotic phosphorylation. *Proc. Natl. Acad. Sci. USA* **105**, 10762–10767.
- Desai, R., Sarpal, R., Ishiyama, N., Pellikka, M., Ikura, M. and Tepass, U. (2013). Monomeric  $\alpha$ -catenin links cadherin to the actin cytoskeleton. *Nat. Cell Biol.* **15**, 261–273.
- Drees, F., Pokutta, S., Yamada, S., Nelson, W. J. and Weis, W. I. (2005). Alpha-catenin is a molecular switch that binds E-cadherin-beta-catenin and regulates actin-filament assembly. *Cell* **123**, 903–915.
- Dupre-Crochet, S., Figueroa, A., Hogan, C., Ferber, E. C., Bialucha, C. U., Adams, J., Richardson, E. C. and Fujita, Y. (2007). Casein kinase 1 is a novel negative regulator of E-cadherin-based cell-cell contacts. *Mol. Cell Biol.* **27**, 3804–3816.
- Groth, A. C., Fish, M., Nusse, R. and Calos, M. P. (2004). Construction of transgenic *Drosophila* by using the site-specific integrase from phage phiC31. *Genetics* **166**, 1775–1782.
- Gunawan, F., Arandjelovic, M. and Godt, D. (2013). The Maf factor Traffic jam both enables and inhibits collective cell migration in *Drosophila* oogenesis. *Development* **140**, 2808–2817.
- Halbleib, J. M., Sääf, A. M., Brown, P. O. and Nelson, W. J. (2007). Transcriptional modulation of genes encoding structural characteristics of differentiating enterocytes during development of a polarized epithelium in vitro. *Mol. Biol. Cell* **18**, 4261–4278.
- Hansen, S. D., Kwiatkowski, A. V., Ouyang, C. Y., Liu, H., Pokutta, S., Watkins, S. C., Volkmann, N., Hanein, D., Weis, W. I., Mullins, R. D. et al. (2013).  $\alpha$ -Catenin actin-binding domain alters actin filament conformation and regulates binding of nucleation and disassembly factors. *Mol. Biol. Cell* **24**, 3710–3720.
- Harris, T. J. (2012). Adherens junction assembly and function in the *Drosophila* embryo. *Int. Rev. Cell Mol. Biol.* **293**, 45–83.
- Harris, T. J. and Tepass, U. (2010). Adherens junctions: from molecules to morphogenesis. *Nat. Rev. Mol. Cell Biol.* **11**, 502–514.
- Hong, S., Troyanovsky, R. B. and Troyanovsky, S. M. (2013). Binding to F-actin guides cadherin cluster assembly, stability, and movement. *J. Cell Biol.* **201**, 131–143.
- Huttlin, E. L., Jedrychowski, M. P., Elias, J. E., Goswami, T., Rad, R., Beausoleil, S. A., Villén, J., Haas, W., Sowa, M. E. and Gygi, S. P. (2010). A tissue-specific atlas of mouse protein phosphorylation and expression. *Cell* **143**, 1174–1189.
- Ishiyama, N., Tanaka, N., Abe, K., Yang, Y. J., Abbas, Y. M., Umitsu, M., Nagar, B., Bueler, S. A., Rubinstein, J. L., Takeichi, M. et al. (2013). An autoinhibited structure of  $\alpha$ -catenin and its implications for vinculin recruitment to adherens junctions. *J. Biol. Chem.* **288**, 15913–15925.
- Ji, H., Wang, J., Nika, H., Hawke, D., Keezer, S., Ge, Q., Fang, B., Fang, X., Fang, D., Litchfield, D. W. et al. (2009). EGF-induced ERK activation promotes CK2-mediated disassociation of alpha-Catenin from beta-Catenin and transactivation of beta-Catenin. *Mol. Cell* **36**, 547–559.
- Kobiak, A. and Fuchs, E. (2004). Alpha-catenin: at the junction of intercellular adhesion and actin dynamics. *Nat. Rev. Mol. Cell Biol.* **5**, 614–625.
- le Duc, Q., Shi, Q., Blonk, I., Sonnenberg, A., Wang, N., Leckband, D. and de Rooij, J. (2010). Vinculin potentiates E-cadherin mechanosensing and is recruited to actin-anchored sites within adherens junctions in a myosin II-dependent manner. *J. Cell Biol.* **189**, 1107–1115.
- Lee, T. and Luo, L. (1999). Mosaic analysis with a repressible cell marker for studies of gene function in neuronal morphogenesis. *Neuron* **22**, 451–461.
- Lien, W. H., Klezovitch, O., Fernandez, T. E., Delrow, J. and Vasioukhin, V. (2006). alphaE-catenin controls cerebral cortical size by regulating the hedgehog signaling pathway. *Science* **311**, 1609–1612.
- Maher, M. T., Mo, R., Flozak, A. S., Peled, O. N. and Gottardi, C. J. (2010). Beta-catenin phosphorylated at serine 45 is spatially uncoupled from beta-catenin phosphorylated in the GSK3 domain: implications for signaling. *PLoS ONE* **5**, e10184.
- Maiden, S. L. and Hardin, J. (2011). The secret life of  $\alpha$ -catenin: moonlighting in morphogenesis. *J. Cell Biol.* **195**, 543–552.
- Marin, O., Meggio, F. and Pinna, L. A. (1994). Design and synthesis of two new peptide substrates for the specific and sensitive monitoring of casein kinases-1 and -2. *Biochem. Biophys. Res. Commun.* **198**, 898–905.
- McEwen, A. E., Maher, M. T., Mo, R. and Gottardi, C. J. (2014). E-cadherin phosphorylation occurs during its biosynthesis to promote its cell surface stability and adhesion. *Mol. Biol. Cell* **25**, 2365–2374.
- Melani, M., Simpson, K. J., Brugge, J. S. and Montell, D. (2008). Regulation of cell adhesion and collective cell migration by hindsight and its human homolog RREB1. *Curr. Biol.* **18**, 532–537.
- Montell, D. J., Yoon, W. H. and Starz-Gaiano, M. (2012). Group choreography: mechanisms orchestrating the collective movement of border cells. *Nat. Rev. Mol. Cell Biol.* **13**, 631–645.
- Niewiadomska, P., Godt, D. and Tepass, U. (1999). DE-Cadherin is required for intercellular motility during *Drosophila* oogenesis. *J. Cell Biol.* **144**, 533–547.
- Nishimura, T. and Takeichi, M. (2009). Remodeling of the adherens junctions during morphogenesis. *Curr. Top. Dev. Biol.* **89**, 33–54.
- Okamura, H., Garcia-Rodriguez, C., Martinson, H., Qin, J., Virshup, D. M. and Rao, A. (2004). A conserved docking motif for CK1 binding controls the nuclear localization of NFAT1. *Mol. Cell Biol.* **24**, 4184–4195.
- Olsen, J. V., Blagoev, B., Gnäd, F., Macek, B., Kumar, C., Mortensen, P. and Mann, M. (2006). Global, in vivo, and site-specific phosphorylation dynamics in signaling networks. *Cell* **127**, 635–648.
- Pignoni, F., Hu, B. and Zipursky, S. L. (1997). Identification of genes required for *Drosophila* eye development using a phenotypic enhancer-trap. *Proc. Natl. Acad. Sci. USA* **94**, 9220–9225.
- Pokutta, S., Drees, F., Takai, Y., Nelson, W. J. and Weis, W. I. (2002). Biochemical and structural definition of the I-afadin- and actin-binding sites of alpha-catenin. *J. Biol. Chem.* **277**, 18868–18874.
- Pulgar, V., Marin, O., Meggio, F., Allende, C. C., Allende, J. E. and Pinna, L. A. (1999). Optimal sequences for non-phosphate-directed phosphorylation by protein kinase CK1 (casein kinase-1) – a re-evaluation. *Eur. J. Biochem.* **260**, 520–526.
- Rangarajan, E. S. and Izard, T. (2013). Dimer asymmetry defines  $\alpha$ -catenin interactions. *Nat. Struct. Mol. Biol.* **20**, 188–193.
- Roura, S., Miravet, S., Piedra, J., Garcia de Herreros, A. and Duñach, M. (1999). Regulation of E-cadherin/Catenin association by tyrosine phosphorylation. *J. Biol. Chem.* **274**, 36734–36740.
- Sarpal, R., Pellikka, M., Patel, R. R., Hui, F. Y., Godt, D. and Tepass, U. (2012). Mutational analysis supports a core role for *Drosophila*  $\alpha$ -catenin in adherens junction function. *J. Cell Sci.* **125**, 233–245.
- Schneider, S., Herrenknecht, K., Butz, S., Kemler, R. and Hausen, P. (1993). Catenins in *Xenopus* embryogenesis and their relation to the cadherin-mediated cell-cell adhesion system. *Development* **118**, 629–640.
- Schober, M., Rebay, I. and Perrimon, N. (2005). Function of the ETS transcription factor Yan in border cell migration. *Development* **132**, 3493–3504.
- Simpson, K. J., Selfors, L. M., Bui, J., Reynolds, A., Leake, D., Khvorova, A. and Brugge, J. S. (2008). Identification of genes that regulate epithelial cell migration using an siRNA screening approach. *Nat. Cell Biol.* **10**, 1027–1038.
- Stappert, J. and Kemler, R. (1994). A short core region of E-cadherin is essential for catenin binding and is highly phosphorylated. *Cell Adhes. Commun.* **2**, 319–327.
- Tamada, M., Farrell, D. L. and Zallen, J. A. (2012). Abl regulates planar polarized junctional dynamics through  $\beta$ -catenin tyrosine phosphorylation. *Dev. Cell* **22**, 309–319.
- Taus, T., Köcher, T., Pichler, P., Paschke, C., Schmidt, A., Henrich, C. and Mechtler, K. (2011). Universal and confident phosphorylation site localization using phosphoRS. *J. Proteome Res.* **10**, 5354–5362.
- Thompson, A. I. and Lees, C. W. (2011). Genetics of ulcerative colitis. *Inflamm. Bowel Dis.* **17**, 831–848.
- Thoreson, M. A., Anastasiadis, P. Z., Daniel, J. M., Ireton, R. C., Wheelock, M. J., Johnson, K. R., Hummingbird, D. K. and Reynolds, A. B. (2000). Selective uncoupling of p120(ctn) from E-cadherin disrupts strong adhesion. *J. Cell Biol.* **148**, 189–202.
- van Veelen, W., Le, N. H., Helvensteijn, W., Blonden, L., Theeuwes, M., Bakker, E. R., Franken, P. F., van Gurp, L., Meijlink, F., van der Valk, M. A. et al. (2011).  $\beta$ -catenin tyrosine 654 phosphorylation increases Wnt signaling and intestinal tumorigenesis. *Gut* **60**, 1204–1212.
- Vasioukhin, V., Bauer, C., Degenstein, L., Wise, B. and Fuchs, E. (2001). Hyperproliferation and defects in epithelial polarity upon conditional ablation of alpha-catenin in skin. *Cell* **104**, 605–617.
- Weis, S., Shintani, S., Weber, A., Kirchmair, R., Wood, M., Cravens, A., McSharry, H., Iwakura, A., Yoon, Y. S., Himes, N. et al. (2004). Src blockade stabilizes a Flk/cadherin complex, reducing edema and tissue injury following myocardial infarction. *J. Clin. Invest.* **113**, 885–894.
- Weiss, E. E., Kroemker, M., Rüdiger, A. H., Jockusch, B. M. and Rüdiger, M. (1998). Vinculin is part of the cadherin-catenin junctional complex: complex formation between alpha-catenin and vinculin. *J. Cell Biol.* **141**, 755–764.
- Xiao, H., Rizzo, A. N., Siegler, J. and Chen, W. (2013). The importance of bronchial epithelial junction integrity in asthma. *J. Allerg. Ther.* **S11**:003.
- Yang, J., Dokurno, P., Tonks, N. K. and Barford, D. (2001). Crystal structure of the M-fragment of alpha-catenin: implications for modulation of cell adhesion. *EMBO J.* **20**, 3645–3656.
- Yao, M., Qiu, W., Liu, R., Efremov, A. K., Cong, P., Seddiki, R., Payre, M., Lim, C. T., Ladoux, B., Mège, R. M. et al. (2014). Force-dependent conformational switch of  $\alpha$ -catenin controls vinculin binding. *Nat. Commun.* **5**, 4525.
- Yonemura, S., Wada, Y., Watanabe, T., Nagafuchi, A. and Shibata, M. (2010). alpha-Catenin as a tension transducer that induces adherens junction development. *Nat. Cell Biol.* **12**, 533–542.
- Zhai, B., Villén, J., Beausoleil, S. A., Mintseris, J. and Gygi, S. P. (2008). Phosphoproteomic analysis of *Drosophila melanogaster* embryos. *J. Proteome Res.* **7**, 1675–1682.